Cell Insight 2 (2023) 100112

Contents lists available at ScienceDirect

Cell Insight

journal homepage: www.journals.elsevier.com/cell-insight

Research Article

# The CHCHD2/Sirt1 corepressors involve in G9a-mediated regulation of RNase H1 expression to control R-loop

Le Li [1], Yequn Wu [1], Kui Dai, Qing Wang, Shiqi Ye, Qipeng Shi, Zhenfei Chen, Yi-Chun Huang, Weiwei Zhao, Lijia Li [*]

*College of Life Sciences, Wuhan University, Wuhan, 430072, China*

## HIGHLIGHTS

- CHCHD2 acts as a repressive transcription factor to negatively regulate RNase H1 expression and boost R-loop accumulation.
- Sirt1 interacts with CHCHD2 and deacetylates it, which functions as a corepressor to suppress RNase H1 expression.
- G9a prevents CHCHD2 and Sirt1 from accessing the *RNase H1* promoter and induces RNase H1 expression.
- More CHCHD2 and Sirt1 are recruited to the *RNase H1* promoter to inhibit *RNase H1* transcription after G9a depletion.

## GRAPHICAL ABSTRACT

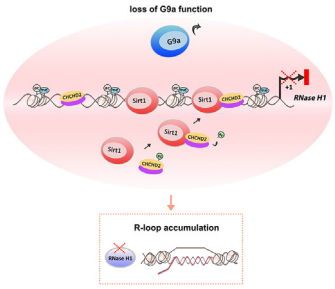


## ARTICLE INFO

*Keywords:*
R-loop
RNase H1
CHCHD2
G9a
Sirt1

## ABSTRACT

R-loops are regulators of many cellular processes and are threats to genome integrity. Therefore, understanding the mechanisms underlying the regulation of R-loops is important. Inspired by the findings on RNase H1-mediated R-loop degradation or accumulation, we focused our interest on the regulation of RNase H1 expression. In the present study, we report that G9a positively regulates RNase H1 expression to boost R-loop degradation. CHCHD2 acts as a repressive transcription factor that inhibits the expression of RNase H1 to promote R-loop accumulation. Sirt1 interacts with CHCHD2 and deacetylates it, which functions as a corepressor that suppresses the expression of downstream target gene *RNase H1*. We also found that G9a methylated the promoter of *RNase H1*, inhibiting the binding of CHCHD2 and Sirt1. In contrast, when G9a was knocked down, recruitment of CHCHD2 and Sirt1 to the *RNase H1* promoter increased, which co-inhibited *RNase H1* transcription. Furthermore, knockdown of Sirt1 led to binding of G9a to the *RNase H1* promoter. In summary, we demonstrated that G9a regulates RNase H1 expression to maintain the steady-state balance of R-loops by suppressing the recruitment of CHCHD2/Sirt1 corepressors to the target gene promoter.

* Corresponding author.
*E-mail address:* ljli@whu.edu.cn (L. Li).
[1] These authors contributed equally to this work.

https://doi.org/10.1016/j.cellin.2023.100112
Received 19 April 2023; Received in revised form 25 May 2023; Accepted 28 May 2023
Available online 4 June 2023

## 1. Introduction

R-loops consist of a nascent RNA transcript, non-coding DNA strand hybrid, and single-stranded coding DNA (Marjorie et al., 1976). R-loops are powerful regulators that play important roles in many cellular processes, including gene expression regulation, transcription termination, DNA repair, telomere maintenance, Okazaki fragment maturation, and immunoglobulin class-switch recombination (Skourti-Stathaki & Proudfoot, 2014). The formation of R-loops as threats impairs DNA replication, triggers DNA damage, and often causes genomic instability (Crossley et al., 2019). R-loops formed during episodes of cellular dysregulation have been linked to several human pathologies such as neurodegenerative diseases and cancer (García-Muse & Aguilera, 2019). It is generally accepted that R-loops are dynamically coupled with transcriptional pausing at gene promoters (Chen et al., 2017) and increased RNAPII pausing is often correlated with increased R-loop levels (Shivji et al., 2018; Zhang et al., 2017), whereas efficient transcription elongation prevents R-loop formation (Edwards et al., 2020). Treatment with an RNAPI transcription inhibitor led to increased R-loop levels at rDNA sites (Zhou et al., 2020). Top1 and RNase H1 are partially functionally redundant in mammalian cells to suppress RNAPI transcription-associated R-loop formation, and RNase H1 is enriched in nucleoli to colocalize with R-loops in cultured human cells (Shen et al., 2017). However, excessive R-loop formation can impede transcriptional elongation (Aguilera & Gómez-González, 2008; Huertas & Aguilera, 2003). The absence of RNase H1 in Top1 depleted *E.coli* or yeast increases the accumulation of RNA/DNA hybrids, which impedes efficient transcription elongation during rRNA synthesis (El Hage et al., 2010; Hraiky et al., 2000).

Genomic profiling has shown that RNA/DNA hybrid structures are prevalent at many sites throughout the genome (Chen et al., 2017, Ginno Paul, Lott Paul, Christensen Holly, Korf, & Chédin, 2012), and dynamic but conserved R-loop structures are associated with specific epigenomic signatures in mammals (Sanz Lionel et al., 2016). Several oncogenes, tumor suppressors, and neurodegenerative disease-related genes are prone to R-loop formation (Wongsurawat et al., 2012). R-loops arising from different sources can be processed via different mechanisms (Petermann et al., 2022). R-loop structures can be removed from the genome using Ribonuclease H (Wahba et al., 2011), topoisomerases (Tuduri et al., 2009) and RNA helicases (Mischo et al., 2011). RNase H is a specialized enzyme that can specifically resolve RNA/DNA hybrids, and nuclear RNA/DNA hybrid levels increase upon RNase H depletion (Parajuli et al., 2017). Although RNase H needs to interact with specific proteins (for example, replication protein A) through different regulatory mechanisms to stimulate its activity, the function of RNase H in controlling R-loop degradation or accumulation is not site-specific (Nguyen et al., 2017). The targets of RNase H activity are possible RNA/DNA hybrids throughout the genome, including the 35S rDNA region transcribed by RNA polymerase I (RNAP I), 5S rDNA transcribed by RNA polymerase III (RNAP III), tRNA genes, retrotransposons, mitochondrial genes, and actively transcribed protein-coding genes in budding yeast genome (El Hage et al., 2014). Significantly, R-loop formation is a natural and frequent event during rRNA transcription (García-Muse & Aguilera, 2019). The rRNA transcription is highly active, and the GC-rich nature of rDNA may promote the generation of R-loops (Chen et al., 2017), which is similar to the 5' pause site of the *β-actin* gene and is a well-characterized RNA/DNA hybrid (Parajuli et al., 2017; Skourti-Stathaki et al., 2014). Loss of RNase H1 also causes RNAP I transcription-associated R-loop accumulation in the nucleus (Shen et al., 2017). Collectively, these lines of evidence demonstrate that RNase H1 plays an important role in the R-loop decomposition, and we chose the rDNA-associated R-loops as the functional readout or reporter locus which were examined following the modulation of RNase H1 expression.

Dimethylated histone H3 lysine 9 (H3K9me2) is a critical epigenetic marker for gene repression and silencing (Tachibana et al., 2008) and plays an essential role in carcinogenesis, aging, and neurodegeneration (Chen et al., 2006; Ding et al., 2013; Yuan et al., 2020; Zheng et al., 2019). Mutation of H3K9me-depositing histone methylation transferase in *Caenorhabditis elegans* may be linked to increased R-loops in repeated genomic elements (Zeller et al., 2016). Fragmented nucleoli are found in *Su(var)* mutant cells, and H3K9 methylation and RNAi pathways are required for normal organization of nucleoli in *Drosophila* (Peng & Karpen, 2007). Our previous study showed that the loss of H3K9me2 caused the augmentation of R-loop accumulation at the rDNA region along with the block of rRNA transcription, which led to nucleoli dispersion (Zhou et al., 2020). G9a (KMT1C, EHMT2) and GLP (KMT1D, EHMT1) are two highly homologous mammalian lysine methyltransferases (KMTs) that form functional heterodimeric complexes that establish monomethylation and dimethylation of histone H3 lysine 9 (H3K9me1 and H3K9me2) in euchromatin, bearing a catalytic SET domain and ankyrin repeats involved in protein–protein interactions and methyl-lysine binding (Battisti et al., 2016; Tachibana et al. 2002, 2005). G9a facilitates transcription complex assembly and rRNA transcription owing to its interaction with RNAP I and promotes changes in epigenetic marks in the rDNA promoter (Yuan et al., 2007). R-loops induce antisense transcription over pause-site termination regions in mammalian protein-coding genes, which leads to the generation of double-stranded RNA and recruitment of DICER, AGO1/2, and G9a. H3K9me2 repressive marks are formed, and heterochromatin protein 1γ (HP1γ) is recruited, which reinforces RNA polymerase II (RNAP II) pausing before efficient transcriptional termination (Skourti-Stathaki et al., 2014). However, the mechanism underlying G9a regulation of R-loop steady-state balance in the human cells requires further elucidation.

Sirt1 is a nicotinamide adenine dinucleotide (NAD+)-dependent deacetylase located mainly in the nucleus and is involved in the regulation of epigenetic modifications, senescence, cancer, and metabolism (Fang et al., 2019; Herskovits & Guarente, 2014; Rahman & Islam, 2011). Sirt1 is critical for chromosome remodeling as it deacetylates lysine residues on histones and acts on some transcription factors and cofactors (Vaquero et al., 2004). In yeast, heterochromatin formation at the ribosomal DNA (rDNA) locus is controlled by the NAD + -dependent deacetylase Sir2p (Buck et al., 2002). A previous study showed that human Sirt1 suppresses pre-rRNA levels in the nucleolus, and nucleoplasmic/nucleolar shuttling is required for Sirt1 to act in the nucleolus (Murayama et al., 2008). Mitotic repression of RNAPI transcription correlates with transient nucleolar enrichment of Sirt1, which deacetylates $TAF_I68$ (another subunit of RNAPI-specific transcription factor SL1). Hypoacetylation of $TAF_I68$ destabilizes SL1 binding to the rDNA promoter, thereby impairing the transcription complex assembly (Voit et al., 2015). In summary, epigenetic control is closely related to Sirt1; however, whether Sirt1 is involved in R-loop regulation in the human cells remains poorly understood.

Coiled-coil-helix-coiled-coil-helix domain-containing protein 2 (CHCHD2), also known as mitochondrial nuclear retrograde regulator 1 (MNRR1), is a multifunctional protein found in both the mitochondria and the nucleus. CHCHD2 plays an important role in regulating mitochondrial metabolism and affects the synthesis of respiratory chain components (Grossman et al., 2017; Meng et al., 2017; Purandare et al., 2018). In mitochondria, CHCHD2 functions in a novel manner by binding to cytochrome *c* oxidase (COX), which stimulates respiration (Aras et al., 2015). In the nucleus, CHCHD2, a transcription factor, transactivates nuclear coding genes and binds to a novel promoter element that contains a highly conserved motif termed the oxygen-responsive element (ORE) in the COX subunit 4 isoform 2 (COX4I2), increasing transcription at 4% oxygen (Aras et al., 2013). In the latest research, a nucleolar long "non coding" RNA encodes a new protein "ribosome IGS coding protein" (RIEP). CHCHD2 and C1QBP, which are known to have mitochondrial and nuclear functions, interact directly with RIEP and relocate following heat shock (Feng et al., 2023). Based on BLAST analysis of the RNase H1 interaction protein databases, we focused on CHCHD2 as an intersection and hypothesized that it may be involved in regulating R-loop degradation or accumulation.

Here, we report a novel transcriptional regulatory function of CHCHD2, which can inhibit the expression of RNase H1, leading to the accumulation of the R-loop. CHCHD2 can form a complex with Sirt1, which binds to the *RNase H1* promoter upon G9a depletion. In contrast, G9a is required for *RNase H1* transcription, mediating H3K9 methylation in the *RNase H1* promoter region, and prevent CHCHD2/Sirt1 co-repressors from binding to the promoter. Collectively, our results revealed that G9a, CHCHD2, and Sirt1 act as regulatory modules for RNase H1 to control R-loop degradation or accumulation.

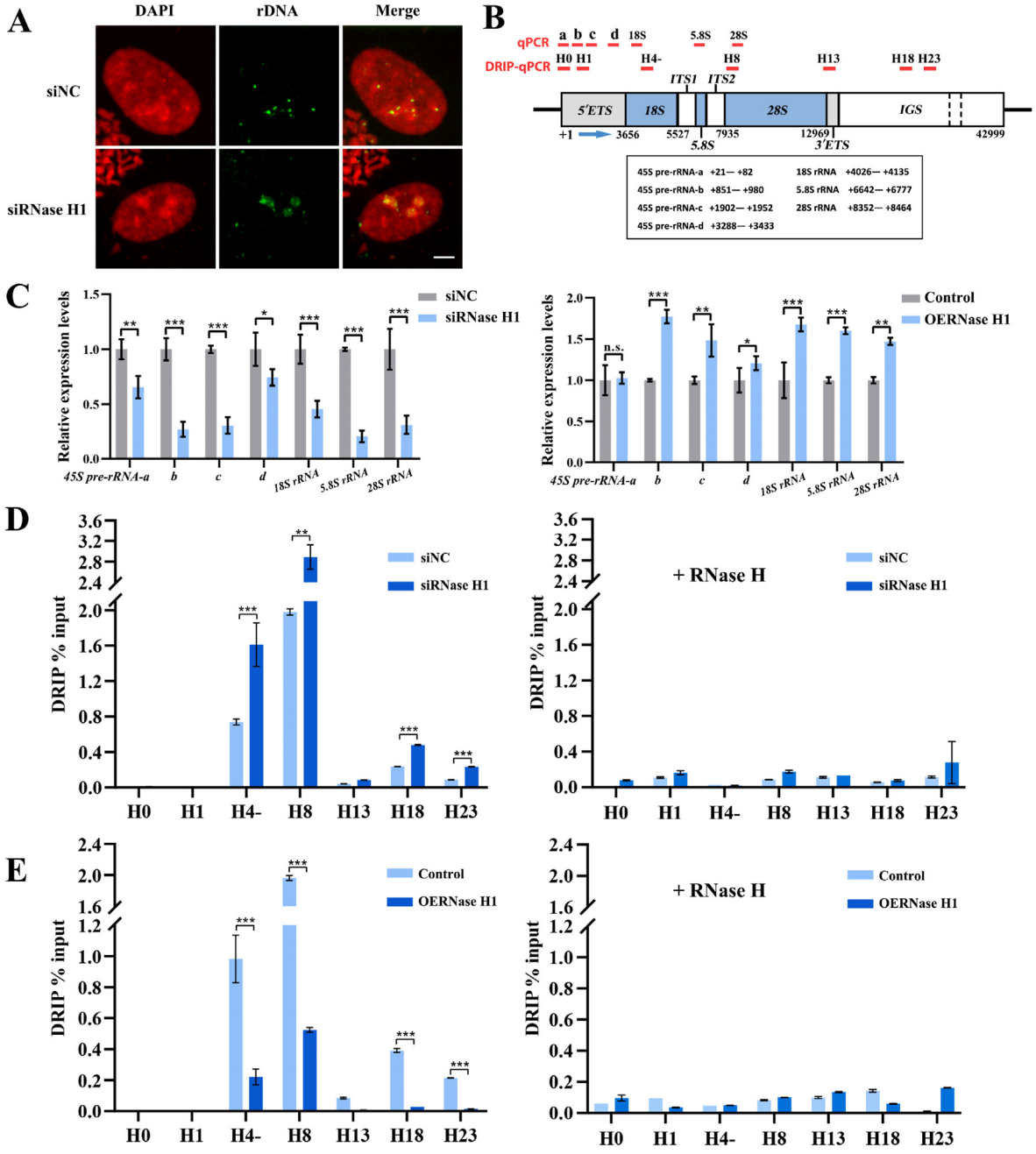


**Fig. 1. The effect of RNase H1 on rDNA decondensation, rRNA transcription, and R-loop degradation or accumulation**

(**A**) Knockdown of RNase H1 caused decondensed rDNA FISH signal patterns in interphase nuclei in HeLa cells. Bar = 3 μm. (**B**) The structure of the human rDNA repeat. The locations of DRIP primer pairs (H0, H1, H4-, H8, H13, H18 and H23) and real-time PCR (qPCR) primers are shown above the diagram of the human rDNA repeat. **(C)** qPCR was used to detect the incomplete 5′ETS transcripts (*45S-pre-rRNA-a, b, c and d*) and the mature rRNA expressions (*18S, 5.8S and 28S*) in HeLa cells after transfection with RNase H1 short-interfering RNA (siRNase H1) and pcDNA3.1-3flag-RNase H1 (OERNase H1) for 48 h. The HeLa cells were used as the control group after transfection with negative control RNA oligo (NC) and the pcDNA3.1-3flag empty vector. Expression values were normalized to the gene *GAPDH*. The relative expression ratio of each sample was compared with untreated cells, expression value of which was assigned as 1. The error bars represent $2^{-\Delta\Delta CT}$ ±SD of three independent experiments. **(D)** DRIP analysis at the rDNA region in HeLa cells with or without in vitro RNase H treatment after transfection with siRNase H1 for 48 h. **(E)** DRIP analysis at the rDNA region in HeLa cells with or without in vitro RNase H treatment after transfection with OERNase H1 for 48 h. The y-axis indicated the ratio of the relative quantities of R-loop in each group. Relative values were normalized to the input. The x-axis indicated different regions of rDNA amplicons. The results represent at least three independent experiments (±SD). All results are expressed as * $P < 0.05$, ** $P < 0.01$, *** $P < 0.001$, n. s. means not significant, measured by the *t*-test.

## 2. Results

### 2.1. RNase H1 is linked to the removal of R-loops in human rDNA

RNase H enzymes are endonucleases that cleave the RNA of RNA/DNA hybrids in a sequence-independent manner (Cerritelli & Crouch, 2009), thus maintaining genome stability by resolving the R-loops formed during transcription (Aguilera & García-Muse, 2012). Our previous studies suggested that the decreased expression of RNase H1 triggered the formation of multiple nucleoli (Zhou et al., 2020) and RNase H1 was implicated in larger rDNA constriction formation (Zhou et al., 2021). Fluorescence *in situ* hybridization (FISH) experiment showed that knockdown of RNase H1 caused decondensed rDNA FISH signal patterns in interphase nuclei of HeLa cells. The rDNA FISH signal was represented as the dense spot in interphase nuclei in normal HeLa cells. In contrast, HeLa cells with the decreased expression of RNase H1 exhibited highly diffused rDNA signals in interphase nuclei (Fig. 1A). After transfection with an appropriate amount of pcDNA3.1-3flag-RNase H1 (OERNase H1) eukaryotic expression plasmid, no highly diffused rDNA signals were observed in interphase nuclei of HeLa cells, and even the signal morphological characteristics were not significantly different from the control group (Supplementary Figure 1A). The results of molecular cytogenetic tests showed that the morphological changes of rDNA were related to RNase H1. In addition, the intrinsic link between R-loop enrichment and transcriptional arrest is more complex than it appears. The qPCR was used to detect the direct effect of RNase H1 on rRNA transcription (Fig. 1B), and our results showed that knockdown of RNase H1 led to the inhibition of rRNA transcription, and overexpression of RNase H1 upregulated rRNA transcription (Fig. 1C, Supplementary Figure 1B). Our analysis of rRNA transcript levels in RNase H1 knockdown or overexpression HeLa cells further confirms that there is a correlation between RNase H1-deletion mediated R-loop enrichment and rRNA transcriptional repression.

The study of R-loops and their degradation has sparked more attention in recent years, where nuclear RNA/DNA hybrid levels have been shown to increase upon human ribonuclease H1 depletion (Parajuli et al., 2017; Shen et al., 2017). To measure the amount of RNA/DNA hybrids in the control group versus the RNase H1-depleted or RNase H1-overexpressed group, we performed DRIP using the well-characterized RNA/DNA hybrid antibody S9.6. We conducted qPCR at the rDNA locus (Fig. 1B), of which the 18S rRNA-coding region (amplicon H4-) and 28S rRNA-coding region (amplicon H8) are the hot spots for R-loop formation, and found that RNase H1 regulates the accumulation of R-loops at a well-characterized hybrid-forming site. Analysis of the DRIP-qPCR signal from RNase H1-depleted cells revealed a significant 2-fold increase in amplicon H4- and a 1.45-fold increase in amplicon H8 in R-loops compared to that in siNC cells (Fig. 1D). As expected, RNase H1-overexpressed cells showed a significant decrease in RNA/DNA hybrids compared with control cells (Fig. 1E). The specificity of the DRIP-qPCR approach was controlled by RNase H treatment in vitro, which compromised the DRIP signal. Expression of RNase H1 was confirmed by Western blot analysis (Supplementary Figure 1C). Further investigation of the role of RNase H1 reveals that RNase H1 activity is linked to the removal of R-loops in human rDNA.

### 2.2. RNase H1 is up-regulated by G9a in a SET-dependent manner

Our previous studies suggested that loss of H3K9 dimethylation (H3K9me2) triggered R-loop accumulation at the rDNA locus, which further led to multilobed nucleoli, indicating that H3K9 methyltransferase G9a is involved in the regulation of R-loop-mediated structural integrity of nucleoli (Zhou et al., 2020). Based on the finding that G9a mediates transcriptional repression as a major epigenetic silencing mechanism (Tachibana et al., 2008), we hypothesized that the role of G9a may directly participate in the regulation of RNase H1 expression. Firstly, puromycin-inducible shRNA was used to generate stable RNA-expressing HeLa cells (like stable shG9a HeLa cells (shG9a), stable shCHCHD2 HeLa cells (shCHCHD2), and stable shSirt1 HeLa cells (shSirt1)), and the shcon HeLa cells (shcon) were generated simultaneously with the same screening conditions of stable shRNA HeLa cells after transfection with pLKO.1 empty vector. Interestingly, we found that knockdown of G9a downregulated *RNase H1* transcription (Fig. 2D), and the result showed a decrease in H3K9me2 and RNase H1 protein levels after transient transfection with G9a short-interfering RNA (siG9a) or pLKO.1-shG9a-#1 (shG9a-#1) in HeLa cells (Fig. 2E). Similar results were obtained in 293T and A549 cells (Supplementary Fig. 2A and B). When we precisely controlled the gradient expression of G9a WT in shcon HeLa cells or stable shG9a HeLa cells, a marked increase in RNase H1 protein level was observed, accompanied by gradient upregulation of G9a WT (Fig. 2F). To explore the relationship between G9a enzyme activity and RNase H1 expression, we used the G9a enzyme-specific inhibitor BIX-01294 (BIX) and another G9a inhibitor BRD4770 (BRD) to inhibit the methyltransferase activity of G9a (Kubicek et al., 2007; Yuan et al., 2012). In this study, we tested the *RNase H1* mRNA level after 48 h of treatment with 10 μM BIX or 10 μM BRD and found that the mRNA level was downregulated (Fig. 2A). Interestingly, when western blotting was used to detect the RNase H1 protein level after 48 h of treatment with different concentrations of BIX or BRD, we found that the RNase H1 protein showed a concentration-dependent decrease (Fig. 2B). After combined treatment with different concentrations of BIX and BRD for 24 h, the level of RNase H1 protein showed a significant decrease, especially in the combined treatment with 5 μM BIX and 10 μM BRD (Fig. 2C). To confirm the importance of G9a HMTase activity in activating RNase H1, we transfected stable G9a knockdown HeLa cells with the G9a WT or G9a ΔSET expression plasmids. We found that the G9a ΔSET group did not show increased RNase H1 expression, whereas the G9a WT group showed increased its expression (Fig. 2G), indicating that the G9a-mediated upregulation of RNase H1 expression is dependent on its HMTase activity. Collectively, these results suggest that G9a positively regulates RNase H1 expression in an SET-dependent manner.

### 2.3. CHCHD2 negatively regulates expression of RNase H1

We identified the co-expressed genes of *RNase H1* from 8 cervical cancer cell lines, and the selected samples are all cervical cancer cell lines included in the Cancer Cell Line Encyclopedia (Broad, 2019) with mRNA experssion data and not profiled for mutation (Ghandi et al., 2019). Select the co-expressed genes of *RNase H1* based on Spearman correlation coefficient and adjusted *p*-value (Cerami et al., 2012; Gao et al., 2013). We found an oxidative stress-related protein CHCHD2 may be associated with RNase H1, and there is a significant negative correlation between the expression of *CHCHD2* and *RNase H1* (Supplementary Figure 3A). Notably, CHCHD2 plays an important role in *trans*-activating nuclear coding genes as transcription factors (Aras et al., 2013), while our results showed that CHCHD2 knockdown led to an increase in *RNase H1* transcription (Fig. 3A). In addition, knockdown of CHCHD2 in stable shG9a cells also caused an increase in *RNase H1* transcription (Fig. 3B). Consistent with the qPCR results, the western blotting results showed that RNase H1 levels increased after knockdown of CHCHD2 (Fig. 3C), whereas RNase H1 expression was repressed by CHCHD2 overexpression (Fig. 3D). When the expression of CHCHD2 was restored in stable shCHCHD2 HeLa cells, RNase H1 protein returned to normal levels (Fig. 3E). In particular, CHCHD2-isoform1 did not affect RNase H1 expression. After overexpressing CHCHD2-isoform2 in shcon HeLa cells, stable shG9a HeLa cells, and G9a WT rescued shG9a HeLa cells, western blotting results indicated that overexpression of CHCHD2-isoform2 further reduced RNase H1 protein levels (Fig. 3F). These results show that CHCHD2 negatively regulates expression of RNase H1.

To further understand the mechanisms underlying *RNase H1* transcriptional regulation by G9a and CHCHD2, we conducted a luciferase reporter assay using the *RNase H1*-promoter-luc reporter system. We first cloned three fragments with different *RNase H1* promoter lengths and

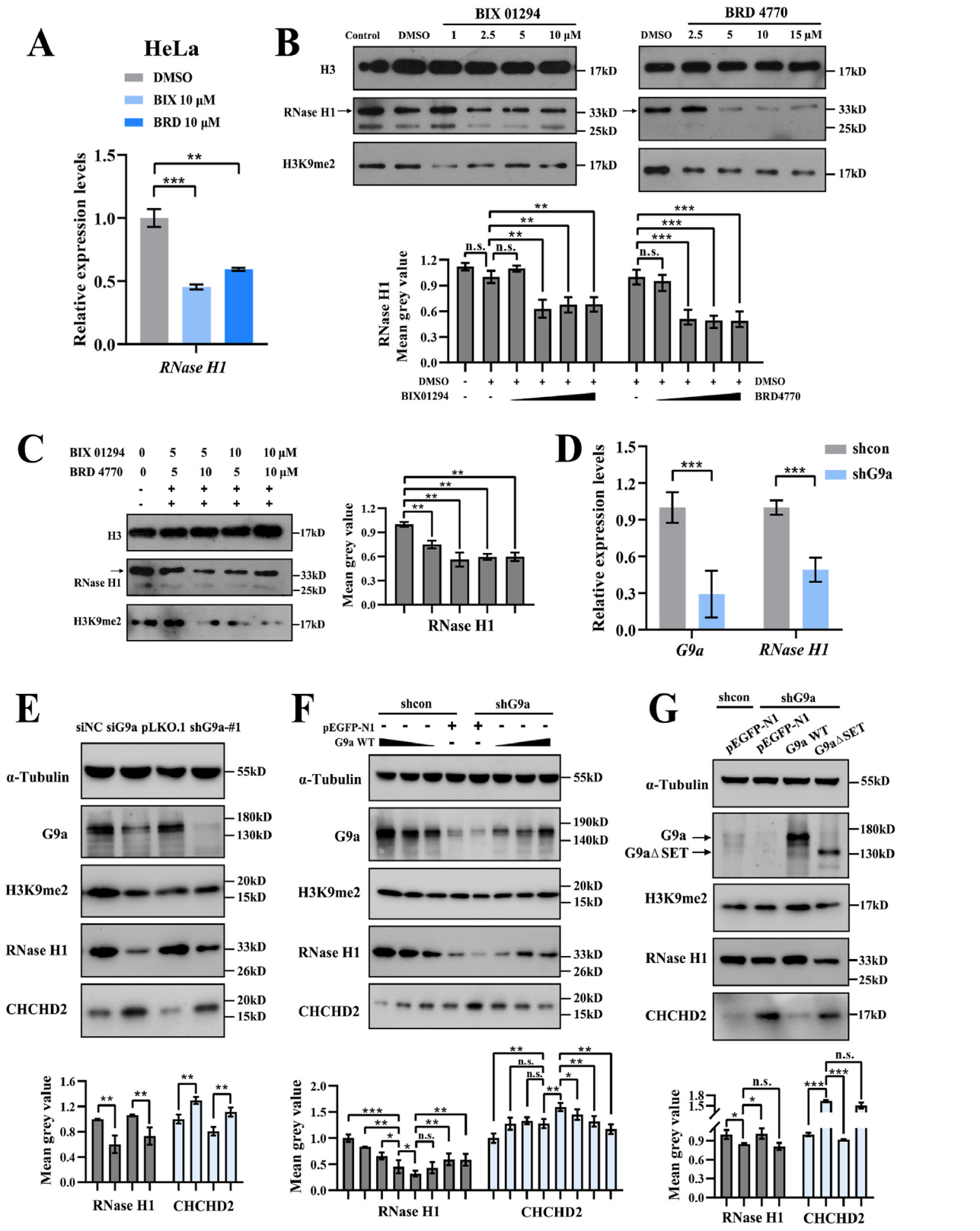


(caption on next page)

**Fig. 2. RNase H1 is up-regulated by G9a in a SET-dependent manner**

**(A)** qPCR was used to detect the *RNase H1* transcription in HeLa cells after treated with 10 μM BIX and 10 μM BRD for 48 h. In the above inhibitor treatment, DMSO was used as the solvent. The same proportion of DMSO as the 10 μM BIX group was used as a solvent control. Expression values were normalized to the gene *GAPDH*. The relative expression ratio of each sample was compared with untreated cells, expression value of which was assigned as 1. The error bars represent $2^{-\Delta\Delta CT} \pm$SD of three independent experiments. **(B)** Western blot analysis of RNase H1 expression and H3K9me2 levels in BIX-treated or BRD-treated (48 h) HeLa cells. **(C)** Western blot analysis of RNase H1 expression in HeLa cells after BIX-BRD combined treatment. In the above inhibitor treatment, DMSO was used as the solvent. The same proportion of DMSO as the 10 μM BIX and the 15 μM BRD group was used as a solvent control. RNase H1 and H3K9me2 levels were quantified to the level of H3. The relative mean gray value of RNase H1 were shown in the lower or right panel. **(D)** qPCR was used to detect the *RNase H1* and *G9a* transcription in shcon HeLa cells and stable shG9a HeLa cells. **(E)** Western blot analysis of RNase H1, CHCHD2, G9a and H3K9me2 expression in HeLa cells after transfection with G9a short-interfering RNA (siG9a) and pLKO.1-shG9a-#1 (shG9a-#1) for 48 h. The HeLa cells were used as the control group after transfection with NC and the pLKO.1 empty vector. **(F)** Western blot analysis of RNase H1, CHCHD2, G9a and H3K9me2 expression in stable shG9a HeLa cells and shcon HeLa cells after transfection with pEGFP-G9a (G9a WT) (0.375, 0.5 and 0.625 μg) for 48 h. The pEGFP-N1 empty vector was used as the negative control and was added to maintain equal amounts of total transfected DNA. **(G)** Western blot analyses showed the relative expression levels of RNase H1, CHCHD2, G9a and H3K9me2 in G9a knockdown HeLa cells, G9a WT and pEGFP-G9a-ΔSET (G9a ΔSET) rescued shG9a HeLa cells. The pEGFP-N1 empty vector was added as the control group. In the above groups, RNase H1, CHCHD2 and G9a levels were quantified to the level of α-tubulin. H3K9me2 levels were quantified to the level of H3 (data not shown). The relative mean gray value of RNase H1 and CHCHD2 were shown in the lower panel. Each experiment was repeated three times, and the average value and SD are shown. Data are expressed as * $P < 0.05$, ** $P < 0.01$, *** $P < 0.001$, and n. s. means no significance, measured by the *t*-test.

engineered these *RNase H1* promoter fragments into pGL3 basic luciferase reporter vectors (Fig. 4A). We selected pGL3-RH1-pro2-luc with the highest promoter activity for the subsequent luciferase assay (Fig. 4B). Consistent with the qPCR and western blotting results, *RNase H1* transcription was stimulated by CHCHD2 depletion and repressed by CHCHD2 overexpression (Fig. 4C). The inhibitory effect of CHCHD2-isoform1 was not as obvious as that of CHCHD2-isoform2. Similarly, we used the *RNase H1*-promoter-luc reporter system to examine the G9a-mediated transcriptional regulation of *RNase H1*. *RNase H1* transcription was repressed by the depletion of G9a and activated by the overexpression of G9a WT but not G9a ΔSET, and BIX treatment attenuated the activation of *RNase H1* transcription triggered by G9a WT (Fig. 4D). After overexpressing CHCHD2-isoform2 in shcon HeLa cells, stable shG9a HeLa cells, and G9a WT rescued shG9a HeLa cells, the results of the relative luciferase activity of *RNase H1* promoter were consistent with the western blotting results (Fig. 3F), indicating that RNase H1 was positively regulated by G9a, and that overexpression of CHCHD2-isoform2 further reduced the expression level of *RNase H1* (Fig. 4E). In contrast, knockdown of CHCHD2 further increased *RNase H1* expression levels compared to those in the control group (Fig. 4F). In addition, we performed an *RNase H1*-promoter-luc reporter assay with stable shCHCHD2 HeLa cells to investigate whether G9a had any effect on the CHCHD2-mediated transcriptional repression of *RNase H1*. Overexpression of G9a abolished *RNase H1* transcriptional repression induced by CHCHD2, and knockdown of G9a further strengthened CHCHD2-mediated *RNase H1* transcriptional repression (Fig. 4G). These results strongly suggest that the negative regulation of *RNase H1* transcription by CHCHD2 is dependent on the depletion of G9a.

Interestingly, knockdown of G9a also resulted in the upregulation of CHCHD2 expression, which further supported the negative regulation of RNase H1 expression by CHCHD2 (Fig. 2E, F, and G; Supplementary Fig. 2A and B). Thus, we conducted a luciferase reporter assay using the *CHCHD2*-promoter-luc reporter system to examine the G9a-mediated transcriptional regulation of *CHCHD2*. We cloned three fragments with different *CHCHD2* promoter lengths and engineered these *CHCHD2* promoter fragments into pGL3 basic luciferase reporter vectors (Supplementary Figure 4A). We selected pGL3-CHCHD2-pro2-luc with the highest promoter activity for the subsequent luciferase assay (Supplementary Figure 4B). The results showed that *CHCHD2* transcription was upregulated by G9a depletion and repressed by G9a overexpression in stable shG9a HeLa cells (Supplementary Figure 4C). Simultan eously, G9a ΔSET did not significantly repress the expression of CHCHD2 compared to G9a WT, indicating that G9a also regulates CHCHD2 in an SET-dependent manner (Fig. 2G , Supplementary Figure 4C).

### 2.4. CHCHD2 is deacetylated by Sirt1

Liquid chromatography matrix assisted laser desorption time-of-flight tandem mass spectrometry (LC MALDI-TOF/TOF MS/MS) analysis identified CHCHD2 as an interacting protein of Sirt1 (Law et al., 2009). The colocalization of CHCHD2 and Sirt1 was also detected by immunofluorescence staining with the CHCHD2 monoclonal antibody (66302-1-Ig) and the Sirt1 polyclonal antibody (07–131) (Fig. 5B). We shifted the Z-axis to display different focal planes and captured images that showed a clear CHCHD2 fluorescence signal in the nuclear region. We quantified the relative signal intensity of co-localizations of CHCHD2 and Sirt1 by a line scan (Fig. 5B), and the experimental results using different species of fluorescent secondary antibodies also showed that CHCHD2 and Sirt1 was partially colocalized in the nucleus of HeLa cells (Supplementary Figure 8A). Nex t, we constructed a yeast two-hybrid system of bait and prey vectors to confirm the direct interaction between Sirt1 and CHCHD2 (Fig. 5A). When using the His antibody or the CHCHD2 antibody to detect GST-Sirt1 pull-down products, a specific band was displayed at a position that was consistent with the size of the input MBP-CHCHD2-His, revealing that both CHCHD2-isoform1 and CHCHD2-isoform2 interacted specifically with Sirt1 in vitro (Fig. 5C). Then, we purified and incubated the recombinant MBP-CHCHD2-His protein and GST-Sirt1 protein to construct a deacetylation reaction system in vitro. A specific band was displayed using the anti-acetylated-lysine antibody at a position that was consistent with the size of input MBP-CHCHD2-His in the GST empty protein reaction products, suggesting that CHCHD2 in the prokaryotic expression system could be acetylated. Compared to the GST empty protein, the addition of GST-Sirt1 significantly reduced the lysine acetylation level of MBP-CHCHD2-His, indicating that Sirt1 directly deacetylated CHCHD2 (Fig. 5E). To further confirm that CHCHD2 was the target of Sirt1-induced deacetylation in vivo, we used stable shSirt1 HeLa cells to perform lysine acetylation immunoprecipitation. Sirt1 knockdown increased the basal acetylation level of endogenous CHCHD2, exogenous CHCHD2-isoform1, and CHCHD2-isoform2. Acetylation could also be restored to the normal level by re-introduction of Sirt1 into stable shSirt1 HeLa cells (Fig. 5D). Collectively, these results suggest that CHCHD2 interacts with Sirt1 and is deacetylated by Sirt1.

### 2.5. Sirt1 functions as a corepressor in CHCHD2-mediated downregulation of RNase H1 expression

Next, we examined whether Sirt1 is involved in the regulation of RNase H1. As expected, *RNase H1* transcription analysis by qPCR showed that treatment with a selective Sirt1 inhibitor EX 527 (Solomon et al., 2006) and transfection with shRNA oligonucleotides (shSirt1-#3) to suppress Sirt1 expression led to a significant increase in *RNase H1* transcription, especially when the inhibitor and shSirt1-#3 were treated together (Fig. 6A). The western blotting results showed that loss of Sirt1 increased RNase H1 expression (Fig. 6B). When we precisely controlled the gradient expression of Sirt1 in shcon HeLa cells or stable shSirt1 HeLa

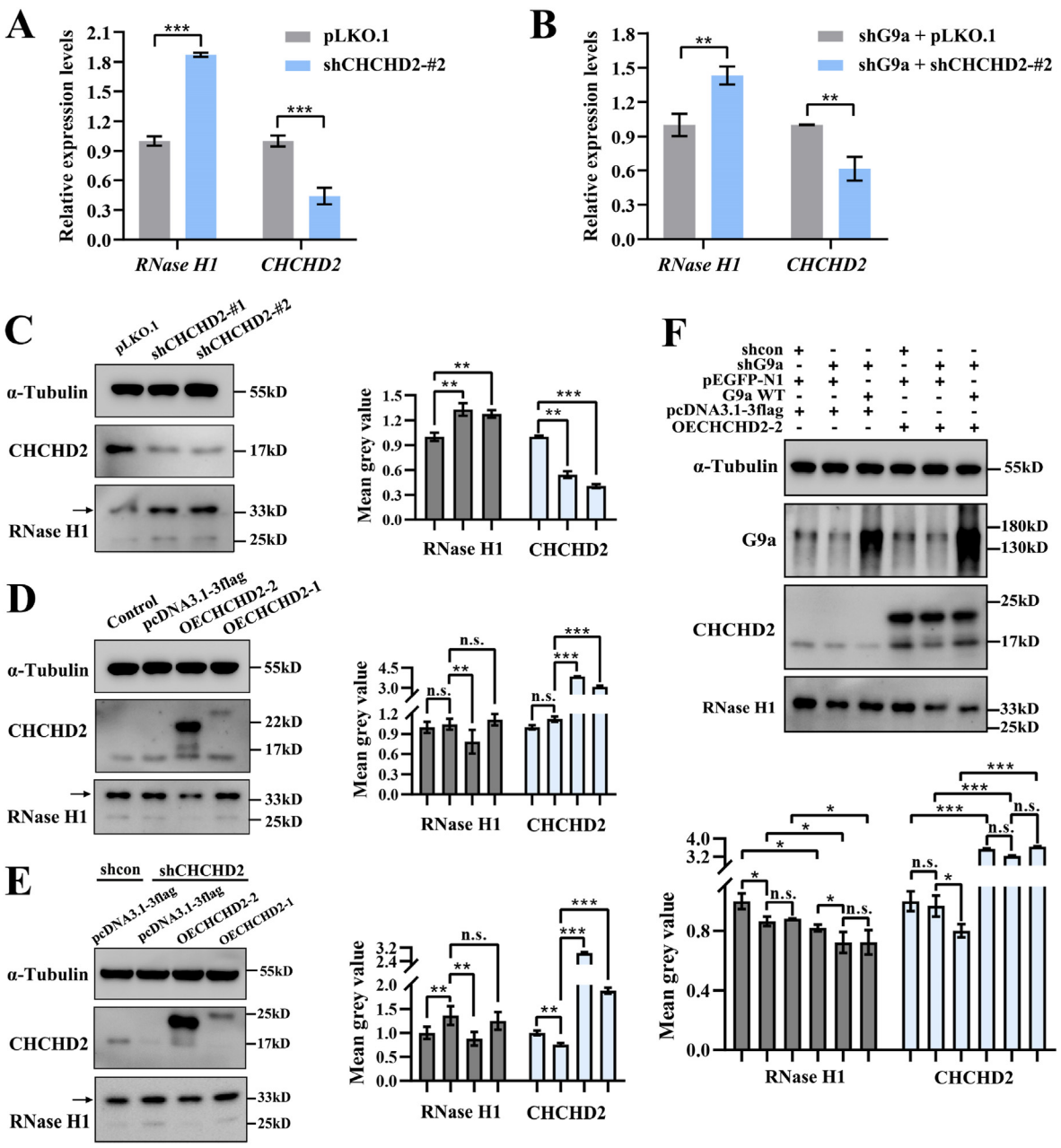


**Fig. 3. CHCHD2 negatively regulates expression of RNase H1**

**(A)–(B)** qPCR was used to detect the *RNase H1* and *CHCHD2* transcription in HeLa cells or stable shG9a HeLa cells after transfection with pLKO.1-shCHCHD2-#2 (shCHCHD2-#2) for 48 h. The pLKO.1 empty vector was added as the control group. Expression values were normalized to the gene *GAPDH*. The relative expression ratio of each sample was compared with untreated cells, expression value of which was assigned as 1. The error bars represent $2^{-\Delta\Delta CT}$ ±SD of three independent experiments. **(C)** Western blot analysis of RNase H1 and CHCHD2 expression in HeLa cells after transfection with pLKO.1-shCHCHD2-#1 (shCHCHD2-#1) and shCHCHD2-#2 for 48 h. **(D)** Western blot analysis of RNase H1 and CHCHD2 expression in HeLa cells after transfection with pcDNA3.1-3flag-CHCHD2-isoform1(OECHCHD2-1) or pcDNA3.1-3flag-CHCHD2-isoform2 (OECHCHD2-2) for 48 h. **(E)** Western blot analyses showed the relative expression levels of RNase H1 and CHCHD2 in CHCHD2 knockdown HeLa cells, CHCHD2-isoform1 and CHCHD2-isoform2 rescued shCHCHD2 HeLa cells. In the above groups, RNase H1 and CHCHD2 levels were quantified to the level of α-tubulin and the relative mean gray value of RNase H1 and CHCHD2 were shown in the right panel. **(F)** Western blot analyses showed the relative expression levels of RNase H1, CHCHD2 and G9a in shcon HeLa cells, stable shG9a HeLa cells and G9a WT rescued shG9a HeLa cells after transfection with OECHCHD2-2 for 48 h. The pEGFP-N1 and the pcDNA3.1-3flag empty vectors were used as the negative control and were added to maintain equal amounts of total transfected DNA. RNase H1, CHCHD2 and G9a levels were quantified to the level of α-tubulin. The relative mean gray value of RNase H1 and CHCHD2 were shown in the lower panel. Each experiment was repeated three times, and the average value and SD are shown. All results are expressed as * $P < 0.05$, ** $P < 0.01$, *** $P < 0.001$, and n. s. means no significance, measured by the *t*-test.

cells, we observed that the level of RNase H1 protein was significantly reduced, accompanied by gradient upregulation of Sirt1 (Fig. 6C , Supplementary Figure 5A). We further used the *RNase H1*-promoter-luc reporter system to examine Sirt1-mediated transcriptional regulation of *RNase H1*. *RNase H1* transcription was repressed by Sirt1 overexpression in stable shSirt1 HeLa cells and treatment with EX 527 attenuated the inhibition of *RNase H1* transcription triggered by Sirt1 (Fig. 6D). Simultaneously, we examined whether CHCHD2 was involved in Sirt1-mediated regulation of RNase H1. Overexpression of CHCHD2-isoform2 in shcon HeLa, stable shSirt1 HeLa, and Sirt1 rescued

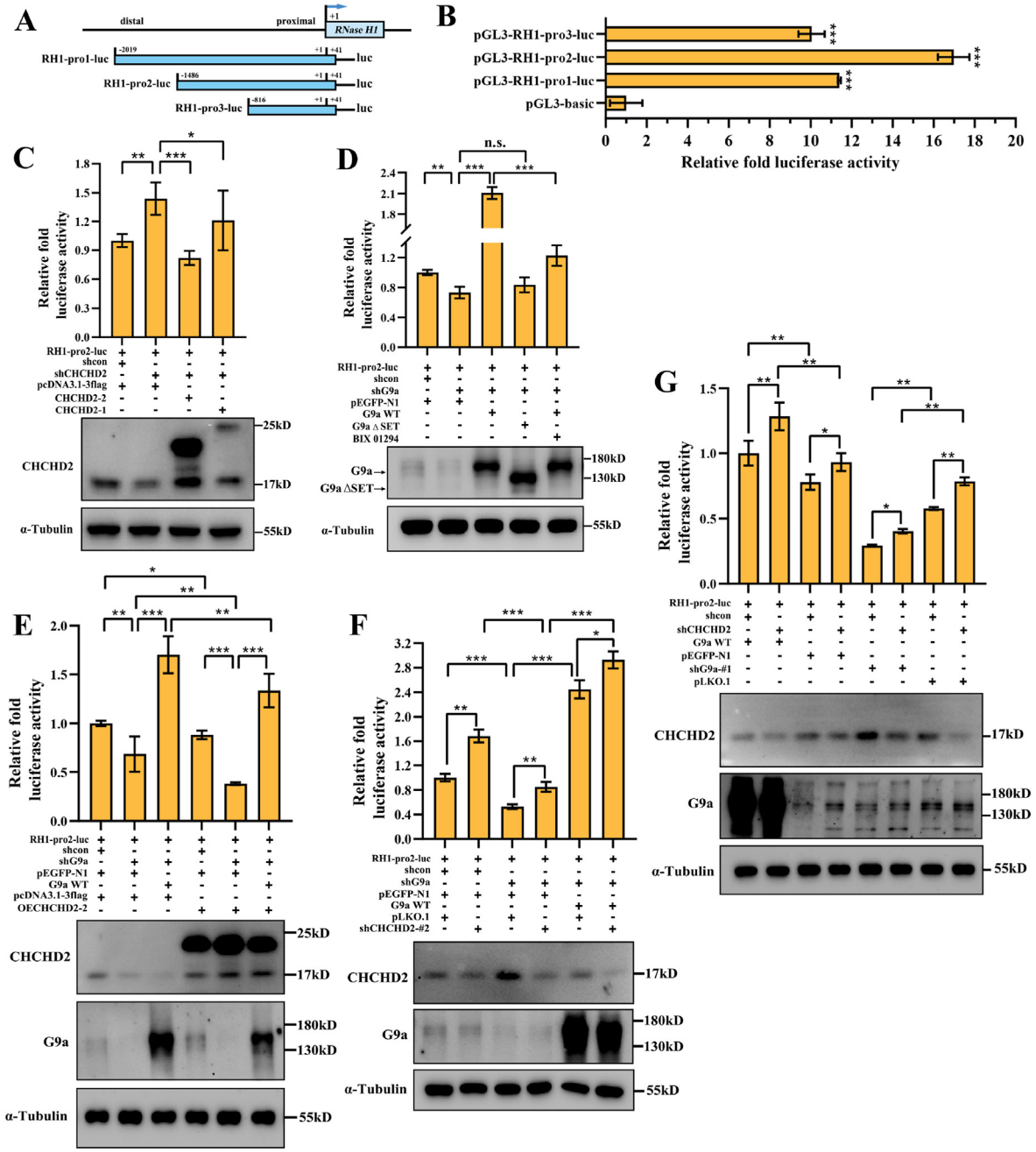


**Fig. 4. G9a and CHCHD2 mediate transcriptional regulation of *RNase H1***

**(A)** Schematic representation of the different lengths of the *RNase H1* promoters (RH1-pro1, RH1-pro2, RH1-pro3), constructed to form the pGL3 luciferase vector. The "+1" represents the transcription start site. **(B)** *RNase H1* promoter activity analysis. **(C)** Stable shCHCHD2 HeLa cells were co-transfected with the pGL3-RH1-pro2-luc (0.75 μg), OECHCHD2-1 (0.5 μg) and OECHCHD2-2 (0.5 μg), along with 0.75 μg TK-Renilla luciferase expression plasmid (pRL-TK). Cell extracts were assayed for luciferase activity. **(D)** Stable shG9a HeLa cells were co-transfected with the pGL3-RH1-pro2-luc (0.75 μg), G9a WT (0.5 μg) and G9a ΔSET (0.5 μg), along with the pRL-TK (0.75 μg). Twenty-four hours after transfection, G9a WT rescued HeLa cells were treated with BIX (10 μM) for 24 h. Cell extracts were assayed for luciferase activity. **(E)** Shcon HeLa cells, stable shG9a HeLa cells and G9a WT rescued shG9a HeLa cells were co-transfected with the pGL3-RH1-pro2-luc (0.75 μg) and OECHCHD2-2 (0.5 μg), along with the pRL-TK (0.75 μg). Cell extracts were assayed for luciferase activity. **(F)** The shcon HeLa cells, stable shG9a HeLa cells and G9a WT rescued shG9a HeLa cells were co-transfected with the pGL3-RH1-pro2-luc (0.75 μg) and shCHCHD2-#2 (0.5 μg), along with the pRL-TK (0.75 μg). Cell extracts were assayed for luciferase activity. **(G)** Shcon HeLa cells and stable shCHCHD2 HeLa cells were co-transfected with the pGL3-RH1-pro2-luc (0.75 μg), G9a WT (0.5 μg) and shG9a-#1 (0.5 μg), along with the pRL-TK (0.75 μg). Cell extracts were assayed for luciferase activity. In the above groups, the pcDNA3.1-3flag, pEGFP-N1, and pLKO.1 empty vector were used as control and were added to maintain equal amounts of total transfected DNA. Expression of the transfected constructs is shown in the immunoblot analysis. Firefly luciferase activity levels were normalized to those of the Renilla luciferases. Each *P*-value represents the mean of three replicates from a single assay. Data are representative of at least three independent experiments and are presented as means ± SD. All the results are expressed as * $P < 0.05$, ** $P < 0.01$, *** $P < 0.001$, and n. s. means no significance, measured by the *t*-test.

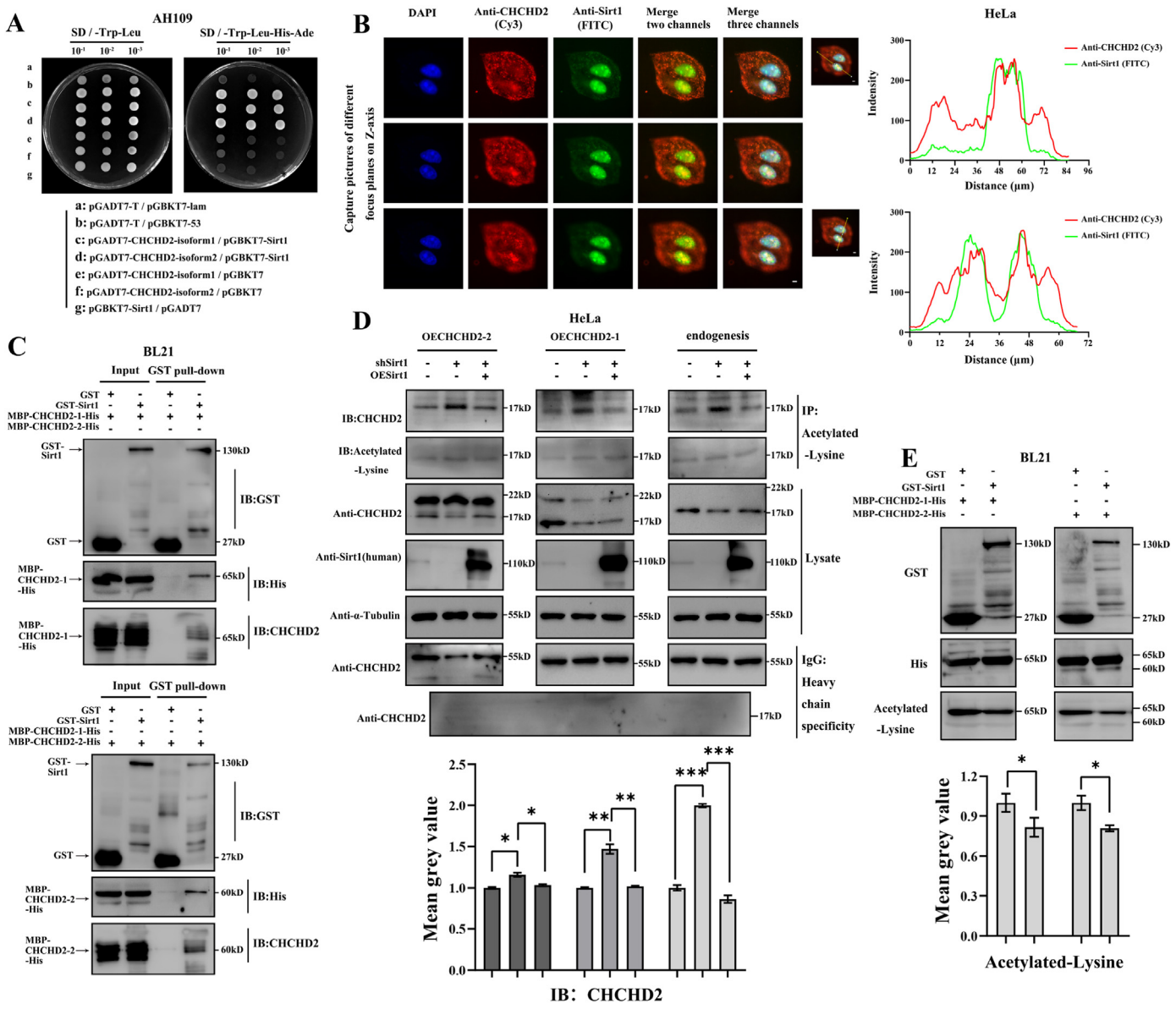


**Fig. 5. CHCHD2 is deacetylated by Sirt1**

**(A)** Detection of the CHCHD2-isoform1/Sirt1 and CHCHD2-isoform2/Sirt1 interactions in a yeast two-hybrid assay. The pGADT7-T and pGBKT7-53 combination was used as a positive control. The pGADT7-T and pGBKT7-lam combination was used as the negative control. **(B)** CHCHD2 and Sirt1 were detected by indirect immunofluorescence staining in interphase nuclei of HeLa cells. From top to bottom, images captured at different focal planes were displayed using secondary antibodies Cy3 Goat Anti-Mouse IgG (H + L) and FITC Goat Anti-Rabbit IgG (H + L). Bar = 5 μm. The relative signal intensity of co-localizations by a line scan were shown in the right panel. **(C)** GST pull-down assay showing the interaction of purified MBP-CHCHD2-His and GST-Sirt1 from BL21. GST-Sirt1 pull-down products were analyzed by western blotting with anti-His and *anti*-CHCHD2 antibodies. **(D)** Upper panel: Acetylation of CHCHD2-isoform1, CHCHD2-isoform2 and endogenous CHCHD2 in stable shSirt1 cells after transfection with pcDNA3.1-3flag-Sirt1 (OESirt1) for 48 h. The pcDNA3.1-3flag empty vector was added as the control group. CHCHD2 acetylation was analyzed by immunoprecipitation with anti-Acetylated-Lysine antibody followed by western blotting for CHCHD2. Expression of each component were shown in the lysate immunoblot analysis. Immunoblotting results of IgG control group incubated with *anti*-CHCHD2 antibody shown by heavy chain specific secondary antibody. IB: CHCHD2 levels were quantified to the level of IB: Acetylated-Lysine. The relative mean gray value of IB: CHCHD2 were shown in the lower panel. **(E)** Upper panel: In vitro CHCHD2 acetylation assay. Purified MBP-CHCHD2-His was incubated with GST-Sirt1 from BL21, in the absence of acetyl-CoA. CHCHD2 acetylation was analyzed by western blotting using anti-Acetylated-Lysine. Acetylated-Lysine levels were quantified to the level of His. The relative mean gray value of Acetylated-Lysine were shown in the lower panel.

shSirt1 HeLa cells. Western blotting results indicated that CHCHD2-isoform2 could further reduce the protein level of RNase H1 (Supplementary Figure 5B), suggesting that CHCHD2 cooperated with Sirt1 to inhibit the expression of RNase H1. Previous studies have shown that non-acetylatable K–R CHCHD2 (all three lysine residues replaced by arginine) is a superior *trans*-activator for activating the COX4I2 promoter luciferase reporter, and the Sirt1 agonist increases this transactivation by CHCHD2 (Aras et al., 2020). Although the above studies clearly show different functions of CHCHD2, further elucidation of whether Sirt1-mediated CHCHD2 lysine deacetylation is involved in RNase H1 regulation is required. A dual-luciferase reporter assay was performed in stable shCHCHD2 HeLa cells using the *RNase H1* promoter luciferase reporter (Fig. 6E). CHCHD2-KR has all three lysine residues mutated to arginine, mimicking a deacetylated protein, showing transcriptional inhibition of *RNase H1*, specifically at position 119, because deacetylation of the other lysine residues does not affect the inhibition. The

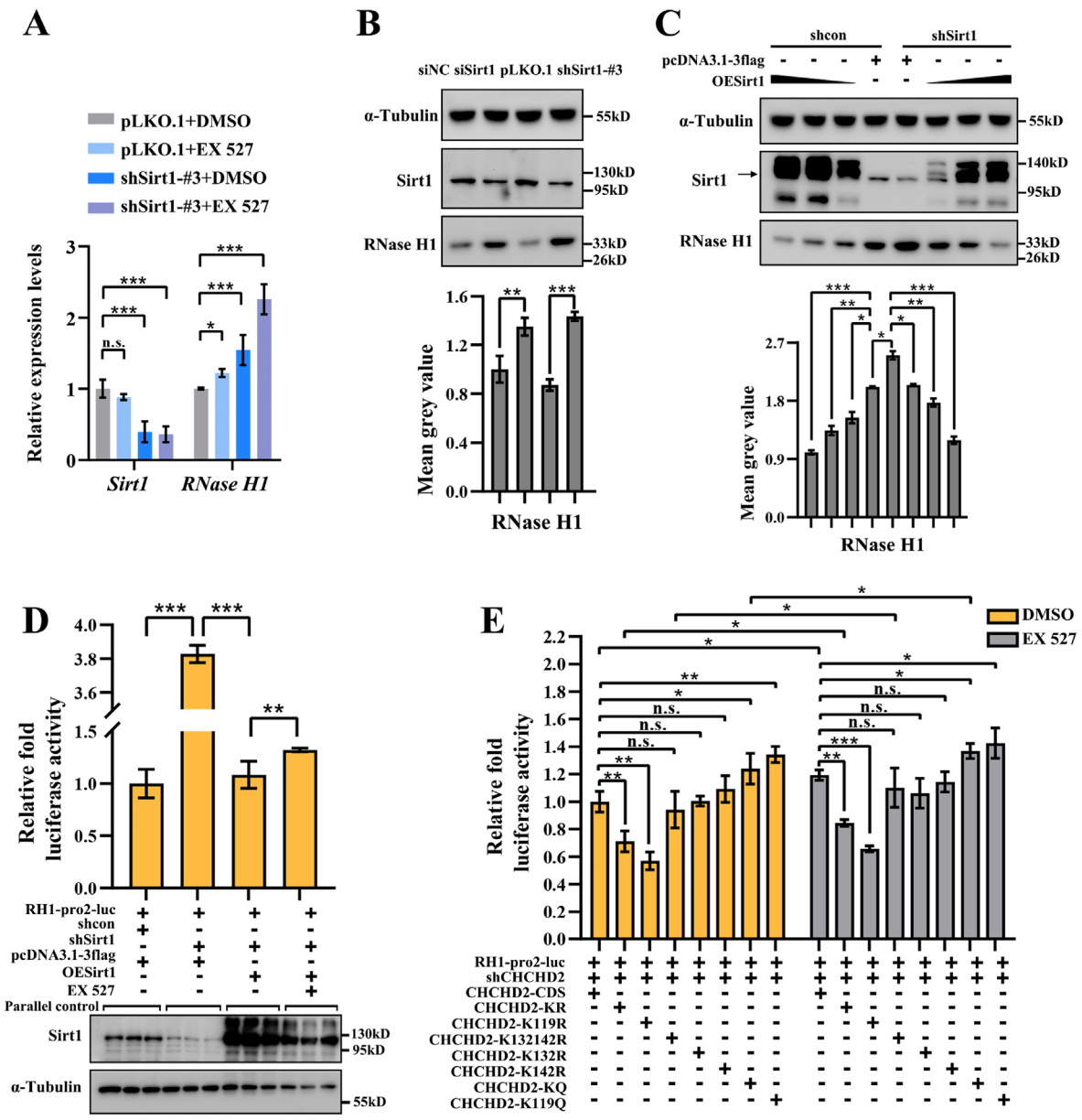


**Fig. 6. Sirt1 functions as a corepressor in regulating RNase H1**

**(A)** qPCR was used to detect the *RNase H1* and *Sirt1* transcription in HeLa cells after treatment with 10 μM EX 527 or transfection with pLKO.1-shSirt1-#3 (shSirt1-#3) for 48 h. The pLKO.1 empty vector was used as the negative control and was added to maintain equal amounts of total transfected DNA. The same proportion of DMSO as the 10 μM EX 527 group were added to the rest of the non-inhibitor treatment group which were used as the solvent control. Expression values were normalized to the gene *GAPDH*. The relative expression ratio of each sample was compared with untreated cells, expression value of which was assigned as 1. The error bars represent $2^{-\Delta\Delta CT}$ ±SD of three independent experiments. **(B)** Western blot analysis of RNase H1 and Sirt1 expression in HeLa cells after transfection with Sirt1 short-interfering RNA (siSirt1) and shSirt1-#3 for 48 h. **(C)** Western blot analysis of RNase H1 and Sirt1 expression in stable shSirt1 HeLa cells and shcon HeLa cells after transfection with OESirt1 (0.375, 0.5 and 0.625 μg) for 48 h. In the above groups, RNase H1 and Sirt1 levels were quantified to the level of α-tubulin. The relative mean gray value of RNase H1 were shown in the lower panel. Each experiment was repeated three times, and the average value and SD are shown. **(D)** Stable shSirt1 HeLa cells were co-transfected with the pGL3-RH1-pro2-luc (0.75 μg), OESirt1 (0.5 μg), along with the pRL-TK (0.75 μg). Twenty-four hours after transfection, Sirt1 rescued HeLa cells were treated with EX 527 (10 μM) for 24 h. The pcDNA3.1-3flag empty vector was used as the negative control and was added to maintain equal amounts of total transfected DNA. The same proportion of DMSO as the 10 μM EX 527 group were added to the rest of the non-inhibitor treatment group which were used as the solvent control. Cell extracts were assayed for luciferase activity. Sirt1 overexpression or knockdown was confirmed by Western blot analysis. **(E)** Stable shCHCHD2 HeLa cells were co-transfected with the pGL3-RH1-pro2-luc (0.75 μg), CHCHD2–isoform2-CDS, -KR, -K119R, -K132142R, -K132R, -K142R, -KQ and -K119Q (0.5 μg), along with 0.75 μg TK-Renilla luciferase expression plasmid (pRL-TK). The pcDNA3.1-3flag empty vector was used as the negative control and was added to maintain equal amounts of total transfected DNA. Cell extracts were assayed for luciferase activity. Firefly luciferase activity levels were normalized to those of the Renilla luciferases. Each *P*-value represents the mean of three replicates from a single assay. Data are representative of at least three independent experiments and are presented as means ± SD. All the results are expressed as * $P < 0.05$, ** $P < 0.01$, *** $P < 0.001$, and n. s. means no significance, measured by the *t*-test.

CHCHD2-KQ mutant, representing an acetyl mimetic (all lysine residues mutated to glutamine), showed superior transactivation ability for the *RNase H1* promoter luciferase reporter, especially K119Q. When treatment with EX 527 caused the Sirt1-induced deacetylation regulatory mechanism in vivo to be out of control, CHCHD2 lost its transcriptional repressor activity, and the transcription level of *RNase H1* was relatively increased compared with the control group.

We then tested the connection between G9a and Sirt1 in influence of RNase H1 expression. The results of *RNase H1*-promoter-luc reporter assay in stable shG9a HeLa cells showed that G9a promoted *RNase H1* transcription; however, overexpression of Sirt1 further abolished *RNase H1* transcriptional activation induced by G9a, and the shSirt1 group showed a significant recovery in *RNase H1* transcriptional repression (Supplementary Figure 6B). Similarly, the results of the *RNase H1*-promoter-luc reporter assay in stable shSirt1 HeLa cells showed that Sirt1 repressed *RNase H1* transcription, but overexpression of G9a slightly recovered Sirt1-mediated transcriptional inhibition of *RNase H1*. Knockdown of G9a further strengthen the Sirt1-mediated *RNase H1* transcriptional repression (Supplementary Figure 6C). In addition, we performed an *RNase H1*-promoter-luc reporter assay in stable shCHCHD2 HeLa cells to investigate whether G9a or Sirt1 had any effect on CHCHD2-mediated transcriptional repression of *RNase H1*. After transfection with OESirt1 or G9a WT for 24 h, shSirt1-#3 or shG9a-#1 was added to the transfection system for an additional 24 h. These results showed that CHCHD2 repressed *RNase H1* transcription. Overexpression of Sirt1 further strengthened CHCHD2-mediated *RNase H1* transcriptional repression. Knockdown of Sirt1 partially restored *RNase H1* transcriptional repression compared to OESirt1, strongly suggesting that Sirt1 is involved in CHCHD2-induced *RNase H1* transcriptional repression (Supplementary Figure 6A). Notably, overexpression of G9a abolished *RNase H1* transcriptional repression induced by CHCHD2, and shG9a further strengthened the transcriptional repression (Fig. 4G, Supplementary Figure 6A).

### 2.6. G9a prevents CHCHD2 and Sirt1 from being recruited to the RNase H1 promoter

To further elucidate the mechanisms underlying *RNase H1* transcriptional regulation by G9a, Sirt1, and CHCHD2, we performed ChIP analysis by qPCR using the corresponding stable knockdown HeLa cells. Histone modification of the *RNase H1* promoter region was discovered using the ChIP-seq public database Cistrome Data Browser. We analyzed the *RNase H1* promoter sequence to identify possible transcription factor-binding sites and designed qPCR primers for ChIP analysis. The final primers RH pro A, B, and C covered the distal, middle, and proximal regions of the *RNase H1* promoter, respectively (Fig. 7A). First, we observed decreased G9a recruitment and decreased levels of H3K9me2 on the *RNase H1* promoter in stable shG9a HeLa cells, whereas G9a was highly recruited to the *RNase H1* promoter and H3K9me2 levels increased when G9a was overexpressed (Fig. 7B). Interestingly, CHCHD2 and Sirt1 recruitment both increased (approximately 2.5- and 3-fold) when G9a was knocked down. Then, we overexpressed G9a in stable shG9a HeLa cells and observed that CHCHD2 and Sirt1 recruitment to the *RNase H1* promoter decreased significantly. H3K9ac levels in the promoter region of *RNase H1* also changed with changes in Sirt1 enrichment (Fig. 7B). These results suggest that high expression G9a prevents CHCHD2 and Sirt1 from accessing the *RNase H1* promoter to activate RNase H1 expression.

Furthermore, in the absence of Sirt1, the H3K9ac level on the *RNase H1* promoter was significantly upregulated, and more G9a was bound to the *RNase H1* promoter, leading to increased levels of H3K9me2. In contrast, overexpression of Sirt1 resulted in a significant reduction in G9a binding and H3K9me2 levels in the *RNase H1* promoter (Fig. 7C). Restoration of Sirt1 expression promoted CHCHD2 enrichment in the *RNase H1* proximal promoter region (RH proC), whereas loss of Sirt1 inhibited the recruitment of CHCHD2. However, no changes in CHCHD2 levels were observed in the *RNase H1* middle promoter region (RH proB) after Sirt1 knockdown (Fig. 7C). These findings demonstrate that Sirt1, CHCHD2, and G9a compete to bind to *RNase H1* promoter regions. Sirt1 cooperated to promote CHCHD2 recruitment only in the proximal region of the *RNase H1* promoter.

### 2.7. G9a, CHCHD2, and Sirt1 are involved in R-loop degradation or accumulation

Under the different modulation profile of RNase H1, we have analyzed the rDNA-associated R-loops, which acted as the functional readout/reporter, to verify the influence of upstream factors on RNase H1 abundance. To investigate the G9a-mediated regulation of R-loop degradation, we performed DRIP analysis of the rDNA region. Compared with the parental cells, shG9a HeLa cells that stably suppressed G9a expression showed a significant increase in R-loop levels at the rDNA locus. In addition, the cells that ectopically expressed G9a wild-type (G9a WT) showed reduced R-loop levels at the rDNA locus; in contrast, SET domain-deleted G9a (G9a ΔSET) failed to repress R-loop accumulation, especially in amplicon H8 (Fig. 8A). Pretreatment with an in vitro RNase H enzyme led to a significant reduction of RNA/DNA hybrids in HeLa cells, confirming the specificity of antibody S9.6. Next, we examined the R-loop levels at the rDNA locus in stable shCHCHD2 HeLa cells, and DRIP-qPCR results confirmed that knockdown of CHCHD2 repressed R-loop accumulation. In contrast, overexpression of CHCHD2-isoform2 increased R-loop accumulation by $>$ 2-fold compared to the control. Overexpression of CHCHD2-isoform1 was less effective than overexpression of CHCHD2-isoform2 in promoting R-loop accumulation at the rDNA site, especially at the amplicon H4- (Fig. 8B). We further observed decreased R-loop levels at amplicon H4-/H8 of the rDNA locus when CHCHD2 was knocked down in stable shG9a HeLa cells (Fig. 8A). As a control for specificity, we pretreated the extracted nucleic acids with RNase H in vitro to degrade existing RNA/DNA hybrids. Collectively, these results suggest that low expression of G9a or high expression of CHCHD2 leads to R-loop enrichment at the rDNA locus, and that CHCHD2 functions downstream of G9a. Furthermore, the DRIP analysis results showed that Sirt1 knockdown reduced the R-loop levels, whereas overexpression of Sirt1 significantly promoted R-loop accumulation, especially in the H4-/H8 rDNA amplicon, which was similar to that obtained from CHCHD2 (Fig. 8C). Pretreatment with RNase H in vitro confirmed the specificity of antibody S9.6. These results suggest that Sirt1 plays the same role as CHCHD2 in regulating R-loop accumulation. Therefore, in this study, we elucidated the effect of the G9a/CHCHD2/Sirt1 regulatory module on RNase H1 expression, and further validated this effect through RNase H1-mediated R-loop removal of rDNA sites.

## 3. Discussion

R-loops are involved in several cellular processes in physiological contexts, such as gene expression, transcription termination, DNA repair, telomere maintenance, Okazaki fragment maturation, and immunoglobulin class-switch recombination (Crossley et al., 2019; Skourti-Stathaki & Proudfoot, 2014). However, R-loops are also considered a double-edged sword, which is a source of replication stress and genome instability causing DNA damage, such as DSBs accumulation (Uruci et al., 2021). RNase H, topoisomerases, and RNA helicases are part of the R-loop degradation machinery associated with the decrease of RNA/DNA hybrids in mammalian cells (Cristini et al., 2018; Parajuli et al., 2017; Song et al., 2017; Yang et al., 2014). However, the exact molecular mechanisms underlying R-loop degradation or accumulation remain unclear. In this study, our findings revealed a novel molecular and genetic mechanism by which the G9a/CHCHD2/Sirt1 regulatory module acts on the expression RNase H1 to control R-loop degradation or accumulation.

Our published article highlights the rDNA FISH signal morphology and corresponding statistical data on metaphase chromosomes after a

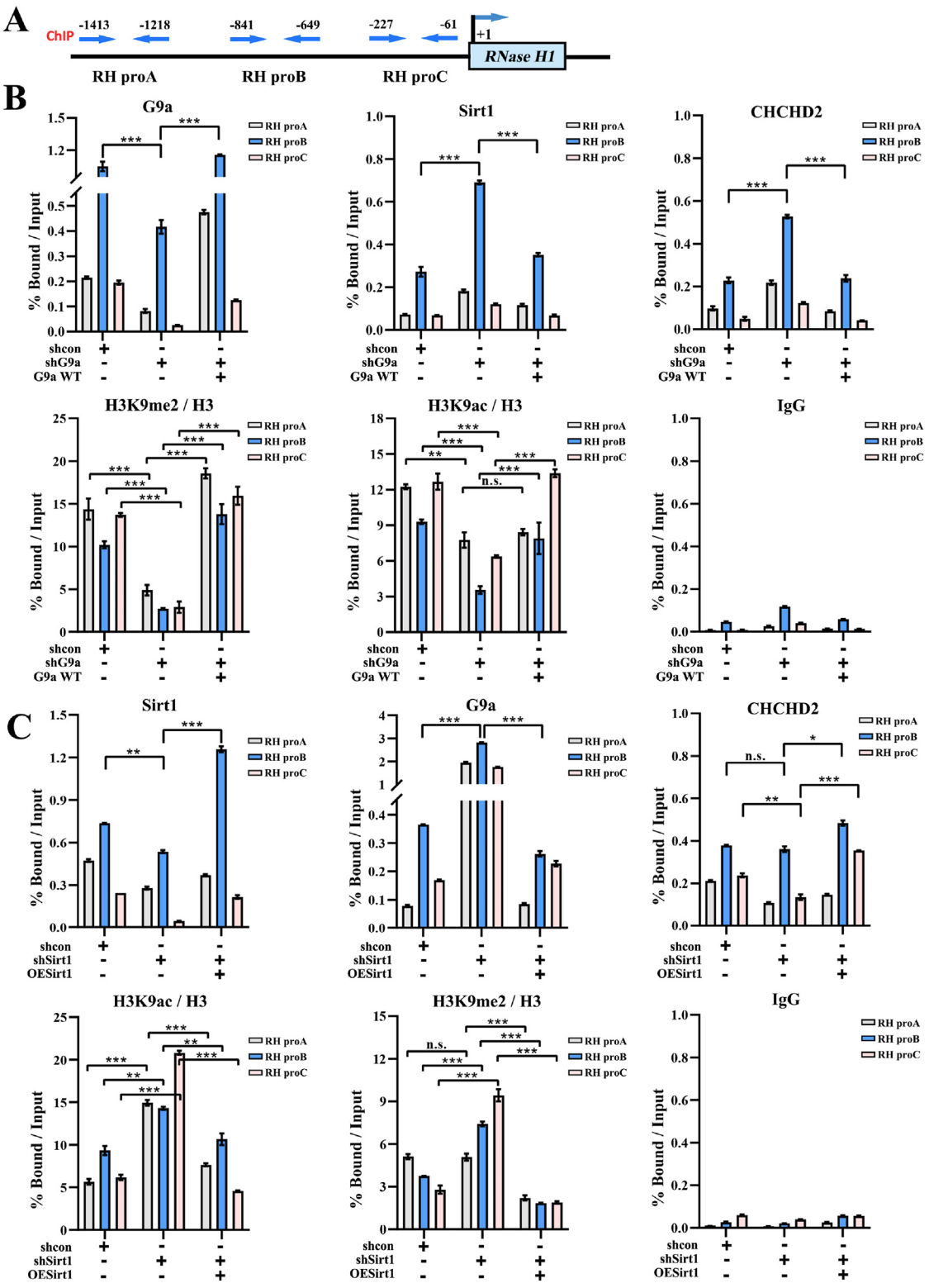


**Fig. 7. G9a prevents CHCHD2 and Sirt1 from being recruited to the *RNase H1* promoter**

**(A)** Schematic diagram of primer pairs in ChIP analysis. Arrows indicate the primers used for qPCR amplification. **(B)** Stable shG9a HeLa cells were transfected with G9a WT. The shcon HeLa cells and stable shG9a HeLa cells which transfect with pEGFP-N1 were used as the control group. ChIP analysis was performed using *anti*-Sirt1, *anti*-G9a, *anti*-CHCHD2, *anti*-H3, *anti*-H3K9ac and *anti*-H3K9me2 antibodies, and the results were confirmed by qPCR. Recruitment of Sirt1, G9a and CHCHD2 to the *RNase H1* promoter was normalized by input. Relative values of H3K9ac and H3K9me2 were normalized to those of the total H3. **(C)** Stable shSirt1 HeLa cells were transfected with OESirt1. The shcon HeLa cells and stable shSirt1 HeLa cells which transfect with pcDNA3.1-3flag were used as the control group. ChIP analysis was performed using *anti*-Sirt1, *anti*-G9a, *anti*-CHCHD2, *anti*-H3, *anti*-H3K9ac and *anti*-H3K9me2 antibodies, and the results were confirmed by qPCR. Recruitment of Sirt1, G9a and CHCHD2 to the *RNase H1* promoter were normalized by input. Relative values of H3K9ac and H3K9me2 were normalized to those of the total H3. All results represent at least three independent experiments (±SD). $^{*}P < 0.05$, $^{**}P < 0.01$, $^{***}P < 0.001$, n. s. means not significant, measured by the *t*-test.

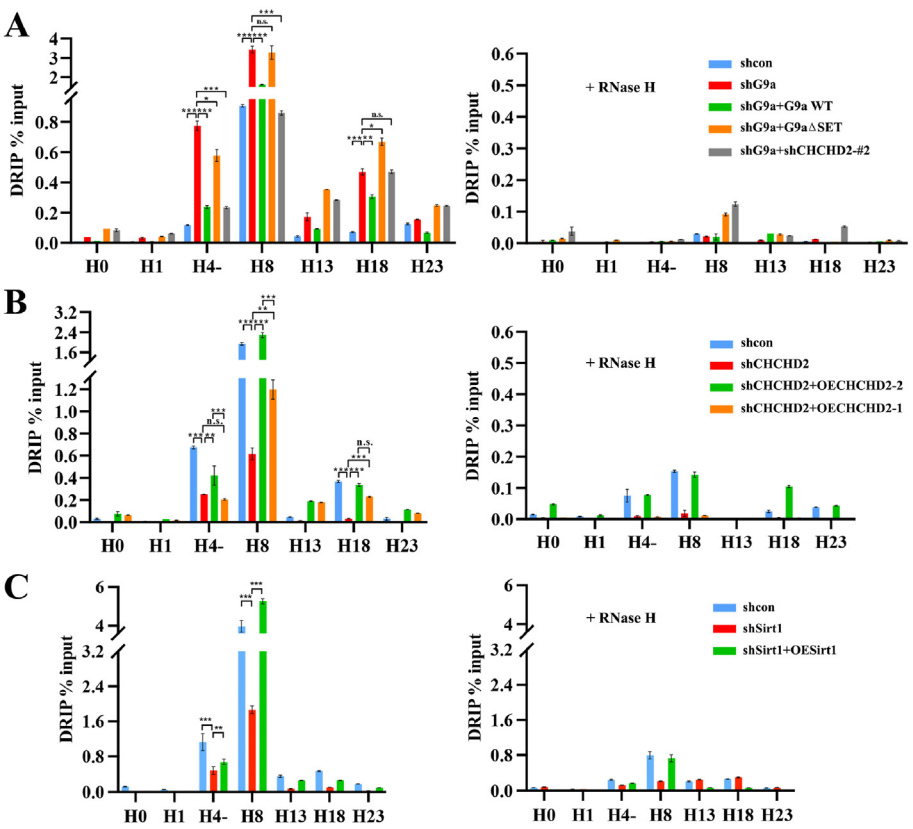


**Fig. 8. The effect of G9a, CHCHD2, and Sirt1 on the R-loop degradation or accumulation**

**(A)** DRIP analysis at the rDNA region in stable shG9a HeLa cells with or without in vitro RNase H treatment after transfection with G9a WT, G9a ΔSET or shCHCHD2-#2 for 48 h. **(B)** DRIP analysis at the rDNA region in stable shCHCHD2 HeLa cells with or without in vitro RNase H treatment after transfection with OECHCHD2-1 or OECHCHD2-2 for 48 h. **(C)** DRIP analysis at the rDNA region in stable shSirt1 HeLa cells with or without in vitro RNase H treatment after transfection with OESirt1 for 48 h. The pEGFP-N1, the pLKO.1 empty vector, and the pcDNA3.1-3flag empty vector were used as the negative control and were added to maintain equal amounts of total transfected DNA. The y-axis indicated the ratio of the relative quantities of R-loop in each group. Relative values were normalized to the input. The x-axis indicated different regions of rDNA amplicons. The above results represent at least three independent experiments and error bars indicate standard deviation (±SD). All results are expressed as * $P < 0.05$, ** $P < 0.01$, *** $P < 0.001$, n. s. means not significant, measured by the *t*-test.

significant decrease or increase in RNase H1 expression level, and confirms the expression level of RNase H1 through Western blot analysis (Zhou et al., 2021). This study takes the morphological characteristics of rDNA on interphase nuclei after changes in RNase H1 expression level as the entry point, and the results of molecular cytogenetic tests showed that the morphological changes of rDNA were closely related to RNase H1. The FISH data we provided in Fig. 1A and Supplementary Figure 1A shared the original data source with our published work (Zhou et al., 2021). After being treated with 0.5 μg/mL Colcemid (Sigma-Aldrich) for a certain period of time, cell mitosis is inhibited, and the proportion of metaphase chromosomes in cells increases. But the produced cell droplets still contain a large number of interphase nuclei. To avoid data duplication, interphase nuclei adjacent to the metaphase chromosome spreads in each experimental group and control group were selected as cytological display objects for the FISH signal morphology of rDNA. It is worth noting that RNase H1 is an endonuclease that specifically hydrolyzes the RNA strand in an RNA/DNA hybrid with limited sequence preference. Therefore, the relationship between human RNase H1 and R-loop regulation involves two processes. First, RNase H1 enhances the recognition of substrates through the *N*-terminal hybrid binding domain (HBD) by increasing the affinity of RNA/DNA hybridization. Second, the HBD is connected to the *C*-terminal catalytic domain (RNase HC) through the free connector required for RNase H1 activity, and the HBD probably anchors the enzyme for multiple rounds of cleavage by RNase HC, leading to increased processivity (Nowotny et al., 2008). At present, R-chip, DRIP, and their improved experimental methods with similar principles can conduct strand-specific and high-resolution localization of R-loops at the whole-genome level, but they only focus on the role of recognizing RNA/DNA hybrid chains. In particular, the R-chip directly mutates RNase HC and retains the function of the HBD, simulating the effect of RNase H1 in recognizing the R-loop under physiological conditions. However, its actual operation requires the construction of a stable RNase H1 mutant cell line; therefore, it cannot objectively reflect the regulatory mechanism of the R-loop after other upstream molecular pathways intervene in RNase H1.

The targets of RNase H activity are possible RNA/DNA hybrids throughout the genome (El Hage et al., 2014). We selected rDNA genes as detection targets because rRNA transcription is highly active, and the GC-rich nature of rDNA may promote the generation of R-loops (Chen et al., 2017), which is similar to the 5' pause site of the *β-actin* gene and is a well-characterized RNA/DNA hybrid (Parajuli et al., 2017; Skourti-Stathaki et al., 2014). In addition, our previous study showed that the loss of H3K9me2 caused the augmentation of R-loop accumulation at the rDNA region along with the repression of rRNA transcription, which led to nucleoli dispersion (Zhou et al., 2020). Owing to the characteristics of tandem repeats of rDNA, genome-wide R-loop detection technologies have mostly been selected to filter out rDNA data to improve resolution (Lin et al., 2022). A feasible method is to use the alignment approach of Zentner et al. to align DRIP-seq reads to the rDNA repeating unit (Nadel et al., 2015; Zentner et al., 2011). In this study, we selected to analyze R-loop enrichment at human rDNA loci by classical relative quantification of DRIP-qPCR, and selected multiple hot spots with RNA/DNA hybridization signatures to increase data coverage. We measured the corresponding R-loop enrichment levels at rDNA sites to further prove the reliability of the changes in RNase H1 abundance after the dynamic alteration of these upstream G9a/CHCHD2/Sirt1 effectors. Further study of the G9a/CHCHD2/Sirt1 effector-mediated changes in R-loop enrichment levels or endogenous RNase H1 recruitment levels in regions other than rDNA genes is required, which will provide meaningful findings from a large amount of data.

The precise regulation of RNase H1 expression is pivotal. RNase H1 is highly evolutionarily conserved and is expressed ubiquitously in human cells and tissues (Wu et al., 1998). There is no significant difference in expression among various human tissues, and it is generally used as a housekeeping gene (Cerritelli & Crouch, 1998). RNase H1 synthesis is subjected to translational regulation, which is affected by two in-frame

AUG codons (M1 and M27) of a single mRNA and a potent upstream open reading frame (uORF) (Suzuki et al., 2010). During normal cell growth and development, RNase H1 expression undergoes sensitive and subtle changes to meet the needs of R-loops to maintain a stable genome level, and subcellular distribution and levels of RNase H1 are fine-tuned in cells to maintain genome integrity (Shen et al., 2017). The aim of this study was to clarify the molecular mechanism underlying changes in RNase H1 abundance, which is dominated by alterations in G9a, Sirt1, and CHCHD2.

G9a and Sirt1 are factors with many downstream targets and pleiotropic phenotypes. The H3K9 HMTase G9a catalyzes the mono- and dimethylation of histone H3K9 and mediates transcriptional repression as a major epigenetic silencing mechanism (Tachibana et al., 2008). One possible mechanism is that G9a and G9a-mediated H3K9me2 act primarily through the recruitment of H3K9me2-binding proteins that prevent transcriptional activation (Scheer & Zaph, 2017). For example, G9a-mediated H3K9 and/or H3K27 monomethylation might then stimulate PRC2 activity and/or recruitment at common genomic loci (Mozzetta et al., 2014), and G9a mediates E4BP4-dependent suppression of hepatic Fgf21 b y enhancing histone methylation (H3K9me2) of the Fgf21 promoter (Tong et al., 2013). It has been reported that G9a is recruited to the UHRF1 promoter along with YY1 to function as a corepressor of the target gene (Kim et al., 2015). The other possible mechanism is that G9a inhibits gene expression by inducing histone hypermethylation at the promoter to prevent the recruitment of transcriptional factors (Roopra et al., 2004). A current research has shown that removal of H3K9me2 by G9a deletion enhances chromatin opening, which facilitate binding of upstream adipogenic transcription factor C/EBPβ to the proximal PPARγ promoter to promote PPARγ expression (Wang et al., 2013). Interestingly, some reports also show that G9a is involved in activation of specific genes in an HMT activity-independent manner (Chaturvedi et al., 2009). Deletion of G9a in preadipocytes decreases Wnt10a expression while inhibiting G9a enzymatic activity has no effect (Wang et al., 2013). G9a has been shown to cooperate with transcription co-activators GRIP1, CARM1 and p300 (Lee et al., 2006). The restriction of G9a methyltransferase activity by histone modifications associated with transcriptional activation could allow G9a to operate as a coactivator (Lee et al., 2006). Thus, G9a plays a dual role in regulating gene expression. Nevertheless, our research results show different G9a regulatory pathways, where G9a positively activates the expression of the target gene *RNase H1* in a SET domain dependent manner, indicating that G9a mediated H3K9me2 on the *RNase H1* promoter might possess corresponding active functions. Our ChIP results demonstrate a weakened accessibility of *RNase H1* promoter after highly histone methylation, resulting in decrease of the binding of CHCHD2 and Sirt1. But the key to our study is that CHCHD2/Sirt1 acts as the transcription inhibitor in the *RNase H1* promoter. Whether the increased H3K9me2 in G9a ectopic expression cells directly recruits other factors to inhibit repressors binding to promote *RNase H1* expression or is simply a marker for the active *RNase H1* promoter remains to be investigated.

Furthermore, we identified a factor, CHCHD2 as a repressor of *RNase H1* transcription. CHCHD2 plays an important role in *trans*-activating nuclear-coding genes as a transcription factor (Aras et al., 2013), regulating mitochondrial metabolism (Aras et al., 2015; Grossman et al., 2017; Purandare et al., 2018) and affecting the synthesis of respiratory chain components (Meng et al., 2017). CHCHD2 contains a mitochondrial targeting sequence at the *N*-terminus, with a transmembrane element in the middle, and a highly conserved CHCH domain carrying a double CX9C motif at the *C*-terminus. CHCHD2 helps neutralize ROS and increase the activity of COX through its CHCH domain (Liu & Zhang, 2015). CHCHD2-isoform1 and CHCHD2-isoform2 come from two different transcriptional variants, respectively. Compared to *CHCHD2* transcriptional variant 2, *CHCHD2* transcriptional variant 1 has the additional 4 bp base in mRNA sequence. In the protein sequence, CHCHD2-isoform1 has a difference of 17aa amino acids at the *C*-terminus compared to CHCHD2-isoform2, with three additional lysine sites. Although both isoforms of CHCHD2 interact with and are deacetylated by Sirt1, the specific deacetylated lysine sites are different. In most relevant studies, the heterotopic expression of CHCHD2 were based on the sequence of isoform 2, so the subsequent research only detected the reporter gene after the single or multiple site mutation of lysine of CHCHD2-isoform2 to determine its inhibitory function. Interestingly, the data we are currently submitting in other journal further explores the additional role of CHCHD2-isoform1 in detail (data not shown). Although the control of the expression of CHCHD2-isoform1 under current conditions does not significantly inhibit the expression of RNase H1, it still plays a certain role in promoting the enrichment of R-loop (Fig. 8B). The possible mechanism is that CHCHD2-isoform1 competitively binds directly to RNA helicase DDX50 and RNase H1, and affects the recruitment of these proteins to R-loop.

Sirt1 can be recruited to gene promoters through direct interactions with sequence-specific transcription factors as well as transcription coregulators. Once present at gene promoters, Sirt1 can modify additional chromatin-associated proteins, including histones, transcription factors, and coregulators, as well as components of the basal transcriptional machinery, to control the activated or inhibited transcription outcome (Feige & Auwerx, 2008). Sirt1 interacts with NCoR and SMRT to repress PPARγ activity (Guarente et al., 2004). Similarly, transcriptional repression by the COUP-TF corepressor, CTIP2, is also enhanced by Sirt1-mediated deacetylation of histones 3 and 4 (Senawong et al., 2003). It is currently unclear whether transcription coregulators are directly deacetylated by Sirt1 or whether promoter specific epigenetic events are triggered that transcription coregulators cooperate with Sirt1 to repress target gene expression through histone deacetylation. In addition, studies have shown that an increase in H3K9ac levels leads to more transcription co regulatory factors binding to target gene promoters, such as HDAC1 silencing led to the occupancy of CBP/p300 to nitric oxide synthase (iNOS) promoter and the rise of H3K9Ac modification (Calegari-Silva et al., 2018). However, the promotion of G9a binding by H3K9ac in the promoter is a novel concomitant phenomenon, and a similar mechanism may be found in current research, where H4K16ac can activate Dot1 histone H3K79 methyltransferase activity (Valencia-Sánchez et al., 2021). The cross-talk regulation between histone modifications and epigenetic modifying enzymes is very complex. Therefore, more exploration is needed to determine whether the increase in histone methyltransferase binding is caused by direct recruitment of H3K9ac or the introduction of other factors that regulate recruitment, and whether the methyltransferase activity of G9a is also promoted. We found that loss of G9a led to the recruitment of more Sirt1 and CHCHD2 to the *RNase H1* promoter to co-inhibit transcription of the *RNase H1* gene. In contrast, the absence of Sirt1 is accompanied by the increase in H3K9ac markers, leading to increased binding of G9a to the *RNase H1* promoter. The enrichment trends of factors in the G9a/CHCHD2/Sirt1 functional module were almost the same for each *RNase H1* promoter region. However, when the expression level of Sirt1 was changed, a significant effect on the recruitment level of CHCHD2 was only manifested in the *RNase H1* proximal promoter region (Fig. 7C). The *RNase H1* distal promoter region was not considered because changes in Sirt1 enrichment and H3K9me2 levels were not significant in the three groups of control experiments. After Sirt1 knockdown, although G9a and corresponding H3K9me2 levels increased, no changes in CHCHD2 levels were observed in the *RNase H1* middle promoter region, possibly due to more complex and unknown regulation of CHCHD2 recruitment and expression.

In summary, this study showed that G9a positively regulates RNase H1 expression and boosts the R-loop degradation, whereas CHCHD2 acts as a repressive transcription factor that inhibits RNase H1 expression to promote R-loop accumulation. CHCHD2 forms a complex with Sirt1 as a corepressor, which binds to the *RNase H1* promoter upon depletion of G9a. This model for responding to changes in RNase H1 abundance is exceptional because it meets the dynamic and sensitive RNase H1 expression requirements to maintain the steady-state balance of R-loops under different physiological conditions. These findings suggest a

possible strategy to regulate R-loop degradation or accumulation and cancer cell growth by co-targeting G9a, CHCHD2, and Sirt1.

## 4. Materials and methods

### 4.1. Drug treatment

BIX-01294 (S8006), BRD4770 (S7591), and EX 527 (S15421) were purchased from Selleck (Shanghai, China) and dissolved in DMSO. Stock solutions were stored at −20 °C and diluted to the respective experimental concentrations with phosphate-buffered saline (PBS) prior to use.

### 4.2. Antibodies

Antibodies specific for RNase H1 (15606-1-AP, Proteintech, Wuhan, China), CHCHD2 (Co-IP:19424-1-AP, Proteintech, Wuhan, China), CHCHD2 (IF & WB:66302-1-Ig, Proteintech, Wuhan, China), G9a (Co-IP: ab183889, Abcam, Cambridge, UK), G9a (WB:66689-1-Ig, Proteintech, Wuhan, China), Sirt1 (07–131, Millipore, USA), α-tubulin (AF0001, Beyotime, Shanghai, China), H3 (AF0009, Beyotime, shanghai, China), H3 (ab1791, Abcam, Cambridge, UK), H3K9ac (ab10812, Abcam, Cambridge, UK), H3K9me2 (ab1220, Abcam, Cambridge, UK), DNA-RNA Hybrid S9.6 (ENH001, Kerafast, Boston, MA, USA), GST (66001-2-Ig, Proteintech, Wuhan, China), His (66005-1-Ig, Proteintech, Wuhan, China), and acetylated-lysine (3067, DIA-AN, Wuhan, China) were used in this study. Other antibodies used were as follows: Cy3 Goat Anti-Mouse IgG (H + L) (A22210, Abbkine, Wuhan, China), FITC Goat Anti-Rabbit IgG (H + L) (A22120, Abbkine, Wuhan, China), Cy3 Goat Anti-Rabbit IgG (H + L) (AP132C, Sigma), and FITC Goat Anti-Mouse IgG (H + L) (F0257, Sigma).

### 4.3. Cell culture

HeLa and 293T cells were purchased from the China Center for Type Culture Collection and cultured in Dulbecco's modified Eagle's medium (DMEM) containing 10% fetal bovine serum (FBS), penicillin (20 units/mL), and streptomycin (20 units/mL). Puromycin (2 μg/mL, P012-25 mg, MDBio, Qingdao, China) was added to the medium for the culture of stable shG9a, shCHCHD2, and shSirt1 cell lines. All cells tested negative for cross-contamination with other human cells and mycoplasma.

### 4.4. Plasmid and transfection

The shRNA oligonucleotides against the target genes G9a, CHCHD2-isoform1, CHCHD2-isoform2, and Sirt1 were cloned into the pLKO.1-TRC cloning vector (Addgene Plasmid 10,878. Protocol Version 1.0. December 2006.). Independent shRNA oligonucleotides were designed with a 5′-*Age*I restriction site overhang on the top strand and a 5′-*Eco*RI restriction site overhang on the bottom strand. Each strand contained a hairpin loop (CTCGAG) and terminator (TTTTT). Puromycin-inducible shRNA was used to generate stable RNA-expressing HeLa cells. HeLa cells were seeded into a 6-well plate until they reached 80%–90% confluence ($2 \times 10^6$) and transfected with 2 μg pLKO.1-shRNA using Lipofectamine 2000(#11668–019, Invitrogen, Carlsbad, California, USA), after which the stably transfected cells were selected in media containing 3 μg/mL of puromycin (P012-25 mg, MDBio, Qingdao, China). The siRNAs against Human RNase H1, Human G9a, Human Sirt1 and the negative control sequence were synthesized by GenePharma (Suzhou, China), and the appropriate siRNA transfection concentration was determined according to the corresponding transfection procedures. The shRNA oligonucleotide and siRNA sequences are listed in Supplementary Table 1.

pEGFP-hG9a (Addgene ID 330025) and pEGFP-ΔSET-hG9a (Addgene ID 330026) plasmids were obtained from Addgene. The full-length coding sequences of the target genes *Sirt1* and *RNase H1* were amplified from human cDNA and cloned into the pcDNA3.1-3flag vector. The CDS sequence of CHCHD2-isoform1 was synthesized by Genewiz (Suzhou, China) and cloned into the pcDNA3.1-3flag vector. The sequence of the CHCHD2-isoform2-CDS was amplified from human cDNA and cloned into the pcDNA3.1-3flag vector. The CHCHD2-isoform2-KR plasmid contained all three lysine residues mutated to arginine, mimicking a deacetylated protein. Similarly, each lysine residue of K119R, K132R, and K142R was mutated, and two lysine residues of K132142R were mutated. The CHCHD2-isoform2-KQ mutant contained all lysine residues mutated to glutamine, representing an acetyl mimetic. Individual lysine residue of K119Q was mutated. The CHCHD2 mutant fragments were designed as previously described (Aras et al., 2020) and constructed into the pcDNA3.1-3flag vector. For each experiment using transient transfection, $2 \times 10^6$ cells were transfected with 2 μg of empty vector or 2 μg of relevant recombinant plasmid. Cells expressing fluorescent tags were counted using a microscope and the transfection efficiency was approximately 55%. For the dual luciferase reporter (DLR) assay, human genomic DNA was prepared, and the resultant *RNase H1* promoter or *CHCHD2* promoter region amplicons were digested with *Kpn*I and *Hin*dIII and inserted into the pGL3-basic vector (Promega). Promoter sequences were amplified using the polymerase chain reaction (PCR) primers listed in Supplementary Table 2. The siRNAs and plasmids were transfected using Gene Twin (#TG101-02, Biomed, Beijing, China) and Lipofectamine 2000 (#11668–019, Invitrogen, Carlsbad, California, USA), respectively, according to the manufacturer's instructions. The activity of the co-transfected Renilla luciferase plasmid (pRL-TK) was used as a transfection efficiency indicator to normalize firefly luciferase activity. The second transfection used the pLKO.1 vector without fluorescent labels, and the transfection effect was reflected by immunoblot analysis. The specific transfection quantity for each recombinant plasmid in the DLR assay is shown in the figure legends. The plasmids for protein interactions: The full-length coding sequences of target genes G9a, CHCHD2-isoform1, CHCHD2-isoform2, and Sirt1 were cloned into pGADT7 or pGBKT7 vectors for yeast two-hybrid experiments. G9a and Sirt1 were cloned into pGEX-4T-1 (with GST tag), and CHCHD2-isoform1 and CHCHD2-isoform2 were cloned into pMAL-C2X vectors (with His tag) for subsequent prokaryotic expression, purification in vitro, and GST pull-down experiments.

### 4.5. Fluorescence in situ hybridization (FISH)

FISH was performed according to a previously reported method (Zhou et al., 2021). Centrifuge and collect the cells in good condition after trypsin digestion, add 2 mL of 0.075 M KCl and hypoosmotic treatment for 30 min at 37 °C, centrifuge at low speed and add 1.5 mL of freshly prepared Carnoy fluid (methanol/acetic acid 3:1) to resuspend the precipitate, centrifuge again and add 1.5 mL of Carnoy fluid to fix the cells for 30min at room temperature, centrifuge and remove the supernatant after fixation. After fixation, the supernatant was removed by centrifugation and 200 μL of Carnoy fluid was added, and the cell suspension was dropped onto a −80 °C pre-cooled no-wash microscope slides from a height of 0.5 m.

The plasmid contains human 5.8S rDNA and 28S rDNA sequences was provided by Dr. Yajuan Li of Dalian Ocean University, DNA probes are digoxigenin-labeled with nick translation. The slides covered with nuclei were immersed in 1% formaldehyde for 3 min and then washed with PBS, transferred to 2 × SSC containing 70% formamide for denaturation at 82 °C for 3 min. After denatured, the slides were dehydrated in 75%, 95%, 100% ethanol for 5 min each and then air-dried it. The hybridization solution containing the appropriate amount of DNA probe (50% deionized formamide, 10% dextran sulfate, 2 μg salmon sperm DNA, 2 × SSC) is denatured at 75 °C for 5 min and then rapidly transferred to ice for 10 min 20 μL of hybridization solution was smeared onto the air-dried slide, incubated in a wet box overnight at 37 °C. Washed slides twice with 2 × SSC, PBS for 5 min each, and then incubated with goat-*anti*-digoxigenin antibody (Roche Molecular Biochem, Basel, Switzerland) at 37 °C for 90 min. After washed with PBS twice for 5 min,

incubated with FITC Rabbit Anti-Goat antibody (Vector Laboratories, Burlingame, CA, USA) at 37 °C for 60 min in the dark. The nuclei after DAPI-stained were examined under a fluorescence microscope equipped with a Cy3, FITC filter.

### 4.6. DNA-RNA immunoprecipitation (DRIP) assay

DRIP assays were performed with some modifications according to the method reported (Ginno Paul et al., 2012; Parajuli et al., 2017). Total nucleic acids were extracted from HeLa cells using sodium dodecyl sulfate (SDS)/proteinase K treatment at 37 °C, followed by phenol-chloroform extraction, isopropanol precipitation and 75% ethanol washing. For RNase H-treated controls, nucleic acids were treated with 75 U/mL RNase H (EN0202, Thermo Scientific, Lithuania) overnight at 37 °C and re-precipitated prior to sonication. Purified DNA was resuspended in 500 μL TE buffer (T1120, Solarbio, Beijing, China) and sonicated with Covaris™ S220 (with settings at Peak Power:100.0, Duty Factor: 5.0, Cycles/Burst:200, and Avg. Power:5.0) for 2 min to generate approximately 250-bp-long DNA sections. Five micrograms of DNA were immunoprecipitated overnight at 4 °C with 5 μg of antibody S9.6 in incubation buffer (20 mM Tris-HCl pH 7.5, 50 mM NaCl, 5 mM ethylenediaminetetraacetic acid [EDTA], 0.2 mM phenylmethylsulphonyl fluoride [PMSF], and 0.2 mM dithiothreitol [DTT]). Immunoprecipitated proteins were bound to rProtein A Sepharose Fast Flow (17-1279-03, GE Healthcare, Uppsala, Sweden) for 3 h, washed thrice in washing buffer (50 mM Tris-HCl pH 7.5, 10 mM EDTA, 50 mM NaCl, 100 mM NaCl, 150 mM NaCl), and then eluted with 50 mM Tris-HCl (pH 7.5), 10 mM EDTA, 50 mM NaCl, 1%SDS, and 20 μg proteinase K for 60 min at 55 °C. Immunoprecipitated DNA was analyzed using real-time PCR using the primers listed in Supplementary Table 3. DNA in the immunoprecipitates was compared with the input DNA, and the difference between untreated and RNase H-treated samples was presented as DRIP signals.

### 4.7. Chromatin immunoprecipitation (ChIP) assay

ChIP was performed according to the method described by Cong et al. (Cong et al., 2012). HeLa ($8 \times 10^5$) cells were washed twice with 1 × PBS after 48 h of transfection, fixed with formaldehyde, and then lysed with 1 mL lysis buffer (1 mM Tris-HCl pH 7.5, 1% SDS, 0.2 mM EDTA, 0.1 mM PMSF, 0.1 mM DTT, 0.1% Protease Inhibitor Cocktail (P8340-1 ML, Sigma)). The genomic DNA dissolved in lysis buffer was sonicated to 500–750-bp sections using ultrasonic fragmentation, of which 40 μL was used as input. The remaining DNA was divided into two samples and added into equal volumes of incubation buffer (consistent with the composition of the incubation buffer used in the DRIP assay), which were blocked with rProtein A Sepharose Fast Flow and Normal Rabbit Serum (BMS0090, Abbkine, Wuhan, China) to remove non-specific antibodies. After centrifugation, the supernatant was incubated overnight at 4 °C with antibody and then bound with protein A for 3 h. IgG-Rb (A7016, Beyotime, Shanghai, China) was used as a negative control for mock immunoprecipitation. The precipitate after centrifugation was washed thrice with a gradient of 1 mL washing buffer (consistent with the composition of the washing buffer used in the DRIP assay), and then eluted with 60 °C preheated elution buffer (20 mM Tris-HCl pH 7.5, 50 mM NaCl, 5 mM EDTA, 0.2 mM PMSF, 0.2 mM DTT, and 1% SDS). The resulting eluate was incubated with 200 mM NaCl and 20 μg of proteinase K at 55 °C for 6 h for decrosslinking, followed by 20 μg of RNase A for 30 min at 37 °C. DNA was then precipitated according to the DNA purification procedure, and the precipitate was subjected to real-time PCR using the primers shown in Supplementary Table 3.

### 4.8. Real-time PCR (qPCR)

RNA extraction and qPCR were performed according to a previously reported method (Zhou et al., 2020). Briefly, cells cultured in six-well plates were digested and lysed with 1 mL TRIzol per well, followed by extraction. The RNA sample was dissolved in RNA-enzyme-free double-distilled water and frozen at −80 °C for subsequent experiments. Total RNA was reverse-transcribed to cDNA using the HiScript® II 1st Strand cDNA Synthesis Kit (R212-01/02, Vazymes, Nanjing, China), which was used as a template for real-time fluorescence quantification using iTaq Universal SYBR® Green Supermix (#1725124, Bio-Rad, California, USA) in a StepOne Plus real-time PCR system (Applied Biosystems, Carlsbad, California, USA). The amplification conditions were 95 °C for 2 min, 95 °C for 5 s, 59 °C for 15 s, and 72 °C for 20 s; and the last three steps were performed for 40 cycles. The quantification control gene was *GAPDH*, and the primers are shown in Supplementary Table 4.

### 4.9. Western blot analysis

Total proteins extracted from the treated cells using extraction buffer (100 mM Tris-HCl pH 7.5, 50 mM NaCl, 5 mM EDTA, 1 mM PMSF, and 1 mM DTT) were separated using SDS-polyacrylamide gel electrophoresis (PAGE). Then the proteins were transferred to polyvinylidene fluoride (PVDF) membranes, blocked with 5% milk at room temperature for 2 h, and incubated overnight at 4 °C with the antibodies. Immunoreactive bands were visualized using chemiluminescence after binding to the corresponding secondary antibody. The secondary antibodies were horseradish peroxidase (HRP)-labeled goat anti-mouse IgG (A0216, Beyotime, Shanghai, China) and the HRP labeled goat anti-rabbit IgG (A0208, Beyotime, Shanghai, China). Immunoreactivity was determined using the ECL method (K-12045-D50, Advansta, California, USA), according to the manufacturer's instructions (Zhou et al., 2021).

### 4.10. Luciferase reporter assays

The promoter of the target gene was cloned into the pGL3 plasmid with the firefly luciferase gene, and the plasmid pRL-TK with the Renilla luciferase gene was used as a control to co-transfect cells with the reporter gene. Total protein was obtained by lysing the cells with lysis solution using a dual fluorescence assay kit (E1910, Promega, Madison, USA). The firefly fluorescence signal was first generated when Luciferase Assay Reagent II was added through an automatic sample injection system after quantifying the intensity of firefly fluorescence. The Stop&Glo Reagent was added to the same sample to quench the above reaction and simultaneously initiate the Renilla luciferase reaction for a second measurement. The ratio obtained from the two measurements in the Spectramax ID5 multi-mode microplate reader (Molecular Devices, California, USA) was used for further analysis. The activity of the co-transfected TK-Renilla luciferase plasmid was used as a transfection efficiency indicator to normalize the firefly luciferase. Extracts from at least three independent transfection experiments were assayed in triplicate. The results are shown as mean ± SD (Farr & Roman, 1992; Sherf et al., 1996).

### 4.11. Immunofluorescence staining

Immunofluorescence staining was performed as previously described (Zhou et al., 2020). Cells cultured on slides were washed with 1 × PBS to remove the medium, fixed with 4% paraformaldehyde for 10 min, washed thrice with 1 × PBS, permeabilized with 0.5% Triton X-100 for 25 min, washed thrice with 1 × PBS, blocked with 3% bovine serum albumin (BSA) at room temperature for 1 h, incubated with the antibody overnight at 4 °C, washed thrice with PBS, and then combined with the secondary antibody labeled with Cy3 and FITC for 2 h at 37 °C. The nuclei were detected using 4′,6-diamidino-2-phenylindole (DAPI) staining, and the other fluorescence was observed using a fluorescence microscope equipped with a Cy3, FITC filter.

### 4.12. GST pull-down

The proteins CHCHD2-isoform1 with a His tag, CHCHD2-isoform2 with a His tag, G9a with a GST tag, and Sirt1 with a GST tag were expressed in *Escherichia coli* (BL21) and purified using a His tag protein purification kit (P2226, Beyotime, Shanghai, China) or a GST tag protein purification kit (P2262, Beyotime, Shanghai, China). The GST pull-down assays were performed according to the method reported by Einarson et al. (Einarson et al., 2007). The proteins carrying those two tags were incubated with equal amounts of pull-down binding buffer (50 mM Tris-HCl pH 8.0, 250 mM NaCl, 1 mM EDTA, 1% NP-40, 10 mM $MgCl_2$, 0.2 mM PMSF and 0.2 mM DTT) and 50 μL of BeyoGold ™ GST-tag Purification resin (rinsing thrice in pull-down binding buffer) for 2 h at 4 °C with end-over-end mixing. Centrifuge the samples at 12,000 g for 10 s at 4 °C in a microcentrifuge and wash the beads six times with 1 mL of ice-cold washing buffer (50 mM Tris-HCl pH 8.0, 300 mM NaCl, 1 mM EDTA, 1% NP-40,10 mM $MgCl_2$, 0.2 mM PMSF, and 0.2 mM DTT). The washes were discarded and then detected with antibodies specific for the tag and target protein using Western blot analysis.

### 4.13. Co-IP assay

Co-IP was performed according to a previously described protocol (You et al., 2019). HeLa ($6 \times 10^5$) Cells transfected for 48 h, digested with trypsin, collected, and washed twice with 1 × PBS. These cells were lysed for 2 h with 1.5 mL buffer A (20 mM Tris-HCl pH 8.0, 150 mM NaCl, 5 mM EDTA, 0.5% NP-40, 0.2 mM PMSF, 0.2 mM DTT, and 0.2% Protease Inhibitor Cocktail (P8340-1 ML, Sigma)), centrifuged at 12,000 g for 10 min, and the supernatant was extracted, of which 300 μL was used as input. The remaining supernatant was blocked with 100 μL of rProtein A Sepharose Fast Flow (17-1279-03, GE Healthcare, Uppsala, Sweden) for 2 h. After centrifugation, the supernatant was extracted again and divided into two equal volumes, one with 2–3 μg of the target protein antibody and one with the homologous IgG (IgG-Rb (A7016, Beyotime, Shanghai, China), IgG-mouse (Q-6004, DIA-AN, Wuhan, China)) as negative control, and mixed overnight at 4 °C in an inverted shaker. Next, 50 μL of rProtein A Sepharose Fast Flow was added to bind to the antibody for 2 h. The antigen-antibody-protein A bead complex was centrifuged at 3000×*g* for 10 min, and the precipitate was washed with 1 mL buffer A and buffer B (20 mM Tris-HCl pH 8.0, 250 mM NaCl, 5 mM EDTA, 0.5% *N*P- 40, 0.2 mM PMSF, 0.2 mM DTT, and 0.2% Protease Inhibitor Cocktail) thrice. The protein bound on the agarose (beads) was eluted with glycine buffer (0.2 M, pH 2.2) for subsequent SDS-PAGE analysis.

### 4.14. In vitro and vivo acetylation detection

Acetylation was detected according to a previously described protocol (You et al., 2019). Sirt1 with GST tag expressed in BL21 were in vitro incubated with the purified CHCHD2-isoform1 and CHCHD2-isoform2 proteins in the deacetylase buffer (10 mM Tris-HCl pH-8.0, 150 mM NaCl, 10% glycerol) for 2 h at 37 °C. Then, the reaction was stopped with stop buffer (1 M HCl, 0.16 M acetic acid). The above components were mixed with equal amounts of loading buffer and separated by electrophoresis on an SDS-PAGE gel. Sirt1 deacetylation was detected by Western blot analysis using the acetylated-lysine antibody (3067, DIA-AN, Wuhan, China). The experimental procedure for in vivo acetylation detection was the same as that used for Co-IP. After knockdown or overexpressing Sirt1 protein in HeLa cells, the cells were lysed in buffer A, and the cell lysate was mixed with acetylated lysine antibodies at 4 °C for overnight, followed by the addition of rProtein A Sepharose Fast Flow. Immunocomplexes were washed with 1 mL of buffer A and 1 mL of buffer B thrice and subjected to western blotting.

### 4.15. Yeast two-hybrid analysis

Yeast two-hybrid analysis was performed according to the Matchmaker GAL4 Two-Hybrid System 3 manufacturer's instructions (Clontech, California, USA). The target genes were constructed into the prey plasmid pGAD-T7 and the bait plasmid pGBK-T7, respectively, and the constructed vectors were co-transformed into *Saccharomyces cerevisiae* strain AH109 using the super yeast transformation kit (SK2401-200, Coolaber, Beijing, China). Transformants were grown on synthetic medium plates (SD medium) lacking Trp and Leu (SD/-Trp-Leu) at 30 °C for 2 d. Colonies with good growth status were selected, diluted with sterile water, and recultured on medium plates (SD/-Trp-Leu-His-Ade).

### 4.16. Statistical analysis

Data and error bars were calculated from three independent experiments. The data in this study were analyzed for significant differences between the experimental and control groups using the *t*-test, which was performed using Microsoft Excel (2019). "Two tails" was used for the calculations of *P* values. "Type 2" was selected for equivariance hypothesis between two groups. Statistical significance was set at $P < 0.05$.

## Availability of data and materials

All data generated or analyzed during this study are included in this published article and its supplementary information files or are available upon request.

## Funding

This work was supported by the National Natural Science Foundation of China (No. 31871238). The funders had no role in the study design, data collection and analysis, decision to publish, or preparation of the manuscript.

## Authors' contributions

Le L., Y.W., K.D., Q.W., S.Y., Q.S., Y.H. performed experiments. L.L., Le L., Y.W., K.D., W.Z. planned and analyzed experiments. Le L., Y.W., Q.W., Z.C. helped with data analysis. L.L., Le L., Y.W. wrote and edited the manuscript. L.L., Le L. conceived the study.

## Declaration of competing interest

The authors declare that they have no competing interests.

## Acknowledgements

Not applicable.

## Appendix A. Supplementary data

Supplementary data related to this article can be found at https://doi.org/10.1016/j.cellin.2023.100112.

## References

Aguilera, A., & García-Muse, T. (2012). R Loops: From transcription byproducts to threats to genome stability. *Molecular Cell, 46*, 115–124.

Aguilera, A., & Gómez-González, B. (2008). Genome instability: A mechanistic view of its causes and consequences. *Nature Reviews Genetics, 9*, 204–217.

Aras, S., Bai, M., Lee, I., Springett, R., Hüttemann, M., & Grossman, L. I. (2015). MNRR1 (formerly CHCHD2) is a bi-organellar regulator of mitochondrial metabolism. *Mitochondrion, 20*, 43–51.

Aras, S., Pak, O., Sommer, N., Finley, R., Jr., Hüttemann, M., et al. (2013). Oxygen-dependent expression of cytochrome c oxidase subunit 4-2 gene expression is

mediated by transcription factors RBPJ, CXXC5 and CHCHD2. *Nucleic Acids Research, 41*, 2255–2266.
Aras, S., Purandare, N., Gladyck, S., Somayajulu-Nitu, M., Zhang, K., et al. (2020). Mitochondrial Nuclear Retrograde Regulator 1 (MNRR1) rescues the cellular phenotype of MELAS by inducing homeostatic mechanisms. *Proceedings of the National Academy of Sciences of the United States of America, 117*, 32056–32065.
Battisti, V., Pontis, J., Boyarchuk, E., Fritsch, L., Robin, P., et al. (2016). Unexpected distinct roles of the related histone H3 lysine 9 methyltransferases G9a and g9a-like protein in myoblasts. *Journal of Molecular Biology, 428*, 2329–2343.
Buck, S. W., Sandmeier, J. J., & Smith, J. S. (2002). RNA Polymerase I propagates unidirectional spreading of rDNA silent chromatin. *Cell, 111*, 1003–1014.
Calegari-Silva, T. C., Vivarini, Á. C., Pereira, R. M. S., Dias-Teixeira, K. L., Rath, C. T., et al. (2018). Leishmania amazonensis downregulates macrophage iNOS expression via histone deacetylase 1 (HDAC1): A novel parasite evasion mechanism. *European Journal of Immunology, 48*, 1188–1198.
Cerami, E., Gao, J., Dogrusoz, U., Gross, B. E., Sumer, S. O., et al. (2012). The cBio Cancer Genomics Portal: An open platform for exploring multidimensional cancer genomics data. *Cancer Discovery, 2*, 401–404.
Cerritelli, S. M., & Crouch, R. J. (1998). Cloning, expression, and mapping of Ribonucleases H of human and mouse related to bacterial RNase HI. *Genomics, 53*, 300–307.
Cerritelli, S. M., & Crouch, R. J. (2009). Ribonuclease H: The enzymes in eukaryotes. *FEBS Journal, 276*, 1494–1505.
Chaturvedi, C.-P., Hosey, A. M., Palii, C., Perez-Iratxeta, C., Nakatani, Y., et al. (2009). Dual role for the methyltransferase G9a in the maintenance of β-globin gene transcription in adult erythroid cells. *P NATL ACAD SCI USA, 106*, 18303–18308.
Chen, L., Chen, J.-Y., Zhang, X., Gu, Y., Xiao, R., et al. (2017). R-ChIP using inactive RNase H reveals dynamic coupling of R-loops with transcriptional pausing at gene promoters. *Molecular Cell, 68*, 745–757.
Chen, H., Yan, Y., Davidson, T. L., Costa, M., & Shinkai, Y. (2006). Hypoxic stress induces dimethylated histone H3 lysine 9 through histone methyltransferase G9a in mammalian cells. *Cancer Research, 66*, 9009–9016.
Cong, R., Das, S., Ugrinova, I., Kumar, S., Mongelard, F., et al. (2012). Interaction of nucleolin with ribosomal RNA genes and its role in RNA polymerase I transcription. *Nucleic Acids Research, 40*, 9441–9454.
Cristini, A., Groh, M., Kristiansen, M. S., & Gromak, N. (2018). RNA/DNA hybrid interactome identifies DXH9 as a molecular player in transcriptional termination and R-Loop-associated DNA damage. *Cell Reports, 23*, 1891–1905.
Crossley, M. P., Bocek, M., & Cimprich, K. A. (2019). R-Loops as cellular regulators and genomic threats. *Molecular Cell, 73*, 398–411.
Ding, J., Li, T., Wang, X., Zhao, E., Choi, J.-H., et al. (2013). The Histone H3 Methyltransferase G9A epigenetically activates the Serine-Glycine synthesis pathway to sustain cancer cell survival and proliferation. *Cell Metabolism, 18*, 896–907.
Edwards, D. S., Maganti, R., Tanksley, J. P., Luo, J., Park, J. J. H., et al. (2020). BRD4 prevents R-Loop formation and transcription-replication conflicts by ensuring efficient transcription elongation. *Cell Reports, 32*.
Einarson, M. B., Pugacheva, E. N., & Orlinick, J. R. (2007). *GST pull-down*. CSH Protocols, 2007: pdb.prot4757.
El Hage, A., Tollervey, D., French, S. L., & Beyer, A. L. (2010). Loss of Topoisomerase I leads to R-loop-mediated transcriptional blocks during ribosomal RNA synthesis. *Genes & Development, 24*, 1546–1558.
El Hage, A., Webb, S., Kerr, A., & Tollervey, D. (2014). Genome-wide distribution of RNA-DNA hybrids identifies RNase H targets in tRNA genes, retrotransposons and mitochondria. *PLoS Genetics, 10*.
Fang, Y., Tang, S., & Li, X. (2019). Sirtuins in metabolic and epigenetic regulation of stem cells. *Trends in Endocrinology and Metabolism, 30*, 177–188.
Farr, A., & Roman, A. (1992). A pitfall of using a second plasmid to determine transfection efficiency. *Nucleic Acids Research, 20*, 920.
Feige, J. N., & Auwerx, J. (2008). Transcriptional targets of sirtuins in the coordination of mammalian physiology. *Current Opinion in Cell Biology, 20*, 303–309.
Feng, S., Desotell, A., Ross, A., Jovanovic, M., & Manley, J. L. (2023). A nucleolar long "non-coding" RNA encodes a novel protein that functions in response to stress. *Proceedings of the National Academy of Sciences of the United States of America, 120*, Article e2221109120.
Gao, J., Aksoy, B. A., Dogrusoz, U., Dresdner, G., Gross, B., et al. (2013). Integrative analysis of complex cancer genomics and clinical profiles using the cBioPortal. *Science Signaling, 6*, pl1. pl1.
García-Muse, T., & Aguilera, A. (2019). R Loops: From physiological to pathological roles. *Cell, 179*, 604–618.
Ghandi, M., Huang, F. W., Jané-Valbuena, J., Kryukov, G. V., Lo, C. C., et al. (2019). Next-generation characterization of the cancer cell line Encyclopedia. *Nature, 569*, 503–508.
Ginno Paul, A., Lott Paul, L., Christensen Holly, C., Korf, I., & Chédin, F. (2012). R-Loop formation is a distinctive characteristic of unmethylated human CpG island promoters. *Molecular Cell, 45*, 814–825.
Grossman, L. I., Purandare, N., Arshad, R., Gladyck, S., Somayajulu, M., et al. (2017). MNRR1, a biorganellar regulator of mitochondria. *Oxidative Medicine and Cellular Longevity*, 1–12.
Guarente, L., Picard, F., Kurtev, M., Chung, N., Topark-Ngarm, A., et al. (2004). Sirt1 promotes fat mobilization in white adipocytes by repressing PPAR-γ. *Nature, 429*, 771–776.
Herskovits, A. Z., & Guarente, L. (2014). SIRT1 in neurodevelopment and brain senescence. *Neuron, 81*, 471–483.
Hraiky, C., Drolet, M., & Raymond, M.-A. (2000). RNase H overproduction corrects a defect at the level of transcription elongation during rRNA synthesis in the absence of DNA topoisomerase I in *Escherichia coli*. *Journal of Biological Chemistry, 275*, 11257–11263.
Huertas, P., & Aguilera, A. (2003). Cotranscriptionally formed DNA:RNA hybrids mediate transcription elongation impairment and transcription-associated recombination. *Molecular Cell, 12*, 711–721.
Kim, K.-B., Son, H.-J., Choi, S., Hahm, J. Y., Jung, H., et al. (2015). H3K9 methyltransferase G9a negatively regulates UHRF1 transcription during leukemia cell differentiation. *Nucleic Acids Research, 43*, 3509–3523.
Kubicek, S., O'Sullivan, R. J., August, E. M., Hickey, E. R., Zhang, Q., et al. (2007). Reversal of H3K9me2 by a small-molecule inhibitor for the G9a histone methyltransferase. *Molecular Cell, 25*, 473–481.
Law, I. K. M., Liu, L., Xu, A., Lam, K. S. L., Vanhoutte, P. M., et al. (2009). Identification and characterization of proteins interacting with SIRT1 and SIRT3: Implications in the anti-aging and metabolic effects of sirtuins. *Proteomics, 9*, 2444–2456.
Lee, D. Y., Northrop, J. P., Kuo, M.-H., & Stallcup, M. R. (2006). Histone H3 lysine 9 methyltransferase G9a is a transcriptional coactivator for nuclear receptors. *Journal of Biological Chemistry, 281*, 8476–8485.
Lin, R., Zhong, X., Zhou, Y., Geng, H., Hu, Q., et al. (2022). R-loopBase: A knowledgebase for genome-wide R-loop formation and regulation. *Nucleic Acids Research, 50*, D303–D315.
Liu, Y., & Zhang, Y. (2015). CHCHD2 connects mitochondrial metabolism to apoptosis. *Molecular & Cellular Oncology, 2*, Article e1004964. e64.
Marjorie, T., Raymond, L. W., & Ronald, W. D. (1976). Hybridization of RNA to double-stranded DNA: Formation of R-loops. *Proceedings of the National Academy of Sciences of the United States of America, 73*, 2294.
Meng, H., Yamashita, C., Shiba-Fukushima, K., Inoshita, T., Funayama, M., et al. (2017). Loss of Parkinson's disease-associated protein CHCHD2 affects mitochondrial crista structure and destabilizes cytochrome c. *Nature Communications, 8*, Article 15500.
Mischo, H. E., Gómez-González, B., Grzechnik, P., Rondón, A. G., Wei, W., et al. (2011). Yeast Sen 1 helicase protects the genome from transcription-associated instability. *Molecular Cell, 41*, 21–32.
Mozzetta, C., Pontis, J., Fritsch, L., Robin, P., Portoso, M., et al. (2014). The histone H3 lysine 9 methyltransferases G9a and GLP regulate polycomb repressive complex 2-mediated gene silencing. *Molecular Cell, 53*, 277–289.
Murayama, A., Ohmori, K., Fujimura, A., Minami, H., Yasuzawa-Tanaka, K., et al. (2008). Epigenetic control of rDNA loci in response to intracellular energy status. *Cell, 133*, 627–639.
Nadel, J., Athanasiadou, R., Lemetre, C., Wijetunga, N. A., Broin, P.Ó., et al. (2015). RNA: DNA hybrids in the human genome have distinctive nucleotide characteristics, chromatin composition, and transcriptional relationships. *Epigenetics & Chromatin, 8*, 1–19.
Nguyen, H. D., Yadav, T., Giri, S., Saez, B., Graubert, T. A., & Zou, L. (2017). Functions of replication protein A as a sensor of R loops and a regulator of RNaseH 1. *Molecular Cell, 65*, 832, 47.e4.
Nowotny, M., Cerritelli, S. M., Ghirlando, R., Gaidamakov, S. A., Crouch, R. J., & Yang, W. (2008). Specific recognition of RNA/DNA hybrid and enhancement of human RNase H1 activity by HBD. *EMBO Journal, 27*, 1172–1181.
Parajuli, S., Teasley, D. C., Murali, B., Jackson, J., Vindigni, A., & Stewart, S. A. (2017). Human ribonuclease H1 resolves R-loops and thereby enables progression of the DNA replication fork. *Journal of Biological Chemistry, 292*, 15216–15224.
Peng, J. C., & Karpen, G. H. (2007). H3K9 methylation and RNA interference regulate nucleolar organization and repeated DNA stability. *Nature Cell Biology, 9*, 25–35.
Petermann, E., Lan, L., & Zou, L. (2022). Sources, resolution and physiological relevance of R-loops and RNA-DNA hybrids. *Nature Reviews Molecular Cell Biology, 23*, 521–540.
Purandare, N., Somayajulu, M., Hüttemann, M., Grossman, L. I., & Aras, S. (2018). The cellular stress proteins CHCHD10 and MNRR1 (CHCHD2): Partners in mitochondrial and nuclear function and dysfunction. *Journal of Biological Chemistry, 293*, 6517–6529.
Rahman, S., & Islam, R. (2011). Mammalian Sirt1: Insights on its biological functions. *Cell Communication and Signaling, 9*, 11–18.
Roopra, A., Qazi, R., Schoenike, B., Daley, T. J., & Morrison, J. F. (2004). Localized domains of G9a-mediated histone methylation are required for silencing of neuronal genes. *Molecular Cell, 14*, 727–738.
Sanz Lionel, A., Hartono Stella, R., Lim Yoong, W., Steyaert, S., Rajpurkar, A., et al. (2016). Prevalent, dynamic, and conserved R-loop structures associate with specific epigenomic signatures in mammals. *Molecular Cell, 63*, 167–178.
Scheer, S., & Zaph, C. (2017). The lysine methyltransferase G9a in immune cell differentiation and function. *Frontiers in Immunology, 8*.
Senawong, T., Peterson, V. J., Avram, D., Shepherd, D. M., Frye, R. A., et al. (2003). Involvement of the histone deacetylase SIRT1 in chicken ovalbumin upstream promoter transcription factor (COUP-TF)-interacting protein 2-mediated transcriptional repression. *Journal of Biological Chemistry, 278*, 43041–43050.
Shen, W., Sun, H., De Hoyos, C. L., Bailey, J. K., Liang, X.-H., & Crooke, S. T. (2017). Dynamic nucleoplasmic and nucleolar localization of mammalian RNase H1 in response to RNAP I transcriptional R-loops. *Nucleic Acids Research, 45*, 10672–10692.
Sherf, B. A., Navarro, S. L., Hannah, R. R., & Wood, K. V. (1996). Dual-Luciferase TM Reporter Assay: An advanced co-reporter technology integrating firefly and renilla luciferase assays. *Promega Notes Magazine*.
Shivji, M. K. K., Renaudin, X., Williams, Ç. H., & Venkitaraman, A. R. (2018). BRCA2 regulates transcription elongation by RNA Polymerase II to prevent R-Loop accumulation. *Cell Reports, 22*, 1031–1039.
Skourti-Stathaki, K., Kamieniarz-Gdula, K., & Proudfoot, N. J. (2014). R-loops induce repressive chromatin marks over mammalian gene terminators. *Nature, 516*, 436–439.

Skourti-Stathaki, K., & Proudfoot, N. J. (2014). A double-edged sword: R loops as threats to genome integrity and powerful regulators of gene expression. *Genes & Development, 28*, 1384–1396.
Solomon, J. M., Pasupuleti, R., Xu, L., McDonagh, T., Curtis, R., et al. (2006). Inhibition of SIRT1 catalytic activity increases p53 acetylation but does not alter cell survival following DNA damage. *Molecular and Cellular Biology, 26*, 28–38.
Song, C., Voit, R., Grummt, I., & Hotz-Wagenblatt, A. (2017). SIRT7 and the DEAD-box helicase DDX21 cooperate to resolve genomic R loops and safeguard genome stability. *Genes & Development, 31*, 1370–1381.
Suzuki, Y., Holmes, J. B., Cerritelli, S. M., Sakhuja, K., Crouch, R. J., et al. (2010). An upstream open reading frame and the context of the two AUG codons affect the abundance of mitochondrial and nuclear RNase H1. *Molecular and Cellular Biology, 30*, 5123–5134.
Tachibana, M., Matsumura, Y., Fukuda, M., Shinkai, Y., & Kimura, H. (2008). G9a/GLP complexes independently mediate H3K9 and DNA methylation to silence transcription. *EMBO Journal, 27*, 2681–2690.
Tachibana, M., Ueda, J., Fukuda, M., Shinkai, Y., Sugimoto, K., et al. (2002). G9a histone methyltransferase plays a dominant role in euchromatic histone H3 lysine 9 methylation and is essential for early embryogenesis. *Genes & Development, 16*, 1779–1791.
Tachibana, M., Ueda, J., Fukuda, M., Shinkai, Y., Takeda, N., et al. (2005). Histone methyltransferases G9a and GLP form heteromeric complexes and are both crucial for methylation of euchromatin at H3-K9. *Genes & Development, 19*, 815–826.
Tong, X., Zhang, D., Buelow, K., Guha, A., Arthurs, B., et al. (2013). Recruitment of histone methyltransferase G9a mediates transcriptional repression of Fgf21 gene by E4BP4 protein. *Journal of Biological Chemistry, 288*, 5417–5425.
Tuduri, S., Crabbé, L., Conti, C., Tourrière, H., Holtgreve-Grez, H., et al. (2009). Topoisomerase I suppresses genomic instability by preventing interference between replication and transcription. *Nature Cell Biology, 11*, 1315–1324.
Uruci, S., Lo, C. S. Y., Wheeler, D., & Taneja, N. (2021). R-loops and its chro-mates: The strange case of Dr. Jekyll and mr. Hyde. *International Journal of Molecular Sciences, 22*.
Valencia-Sánchez, M. I., De Ioannes, P., Wang, M., Truong, D. M., Lee, R., et al. (2021). Regulation of the Dot1 histone H3K79 methyltransferase by histone H4K16 acetylation. *Science, 371*, 363.
Vaquero, A., Scher, M., Lee, D., Erdjument-Bromage, H., Tempst, P., & Reinberg, D. (2004). Human SirT1 interacts with histone H1 and promotes formation of facultative heterochromatin. *Molecular Cell, 16*, 93–105.
Voit, R., Seiler, J., & Grummt, I. (2015). Cooperative action of Cdk 1/cyclin B and SIRT1 is required for mitotic repression of rRNA synthesis. *PLoS Genetics, 11*, 1–17.
Wahba, L., Amon Jeremy, D., Koshland, D., & Vuica-Ross, M. (2011). RNase H and multiple RNA biogenesis factors cooperate to prevent RNA:DNA hybrids from generating genome instability. *Molecular Cell, 44*, 978–988.
Wang, L., Xu, S., Lee, J.-E., Baldridge, A., Grullon, S., et al. (2013). Histone H3K9 methyltransferase G9a represses PPARγ expression and adipogenesis. *EMBO Journal, 32*, 45–59.
Wongsurawat, T., Jenjaroenpun, P., Kwoh, C. K., & Kuznetsov, V. (2012). Quantitative model of R-loop forming structures reveals a novel level of RNA-DNA interactome complexity. *Nucleic Acids Research, 40*, e16. e16.
Wu, H., Lima, W. F., & Crooke, S. T. (1998). Molecular cloning and expression of cDNA for human RNase H. *Antisense and Nucleic Acid Drug Development, 8*, 53–61.
Yang, Y., McBride Kevin, M., Hensley, S., Lu, Y., Chedin, F., & Bedford Mark, T. (2014). Arginine methylation facilitates the recruitment of TOP3B to chromatin to prevent R Loop accumulation. *Molecular Cell, 53*, 484–497.
You, Z., Jiang, W.-X., Qin, L.-Y., Gong, Z., Wan, W., et al. (2019). Requirement for p62 acetylation in the aggregation of ubiquitylated proteins under nutrient stress. *Nature Communications, 10*, 1–14.
Yuan, J., Chang, S.-Y., Yin, S.-G., Liu, Z.-Y., Cheng, X., et al. (2020). Two conserved epigenetic regulators prevent healthy ageing. *Nature, 579*, 118–122.
Yuan, X., Feng, W., Imhof, A., Grummt, I., & Zhou, Y. (2007). Activation of RNA polymerase I transcription by cockayne syndrome group B protein and histone methyltransferase G9a. *Molecular Cell, 27*, 585–595.
Yuan, Y., Wang, Q., Paulk, J., Kubicek, S., Kemp, M. M., et al. (2012). A small-molecule probe of the histone methyltransferase G9a induces cellular senescence in pancreatic adenocarcinoma. *ACS Chemical Biology, 7*, 1152–1157.
Zeller, P., Padeken, J., van Schendel, R., Kalck, V., Tijsterman, M., & Gasser, S. M. (2016). Histone H3K9 methylation is dispensable for *Caenorhabditis elegans* development but suppresses RNA:DNA hybrid-associated repeat instability. *Nature Genetics, 48*, 1385–1395.
Zentner, G. E., Saiakhova, A., Manaenkov, P., Adams, M. D., & Scacheri, P. C. (2011). Integrative genomic analysis of human ribosomal DNA. *Nucleic Acids Research, 39*, 4949–4960.
Zhang, X., Chiang, H.-C., Wang, Y., Zhang, C., Smith, S., et al. (2017). Attenuation of RNA polymerase II pausing mitigates BRCA1-associated R-loop accumulation and tumorigenesis. *Nature Communications, 8*, 1–12.
Zheng, Y., Liu, A., Wang, Z.-J., Cao, Q., Wang, W., et al. (2019). Inhibition of EHMT1/2 rescues synaptic and cognitive functions for Alzheimer's disease. *Brain, 142*, 787–807.
Zhou, H., Li, L., Wang, Q., Hu, Y., Zhao, W., et al. (2020). H3K9 demethylation-induced R-Loop accumulation is linked to disorganized nucleoli. *Frontiers in Genetics, 11*, 43.
Zhou, H., Wang, Y., Wang, Q., Li, L., Hu, Y., et al. (2021). R-loops mediate transcription-associated formation of human rDNA secondary constrictions. *Journal of Cellular Biochemistry, 122*, 1517–1533.